Journal of Pharmaceutical Innovation (2026) 21:415
https://doi.org/10.1007/s12247-026-10573-3

RESEARCH

Optimized Chitosan–Lecithin Nanocarriers for Nose-to-Brain Delivery of Dalfampridine in Multiple Sclerosis: Box–Behnken Design Optimization, and Toxicity Evaluation

Jaghatha Therassama[1] · Justus Oliver Jaslin Edward[2] · Somasundaram Arumugam[3] · Pavazhaviji Pazhani[4] · Jose Prakash Dharmian[1]

Received: 8 November 2025 / Accepted: 5 March 2026

Abstract

Purpose This research aims to develop Nose-to-Brain Delivery of Dalfampridine (4-Aminopyridine) Chitosan–Lecithin Nanoparticles (DFP-CSLCNPs) to improve DFP delivery to the Central Nervous System in multiple sclerosis (MS).

Methods In silico molecular docking studies were performed to evaluate drug-target interactions. Nanoparticles were formulated using a chitosan-lecithin system and optimized through a Box-Behnken experimental design. Key parameters such as particle size, zeta potential, and entrapment efficiency were analyzed. Ex vivo permeation studies were performed using excised nasal mucosa.

Results In-silico docking confirmed CNS relevance, with the strongest binding to 6H24 (−11.2 kcal/mol) and favourable Swiss ADME properties. DFP-CSLCNPs were optimized using a 3-factor Box–Behnken experimental design, which predicted an optimal formulation with a particle size of approximately 142 nm, zeta potential of +24 mV, and entrapment efficiency exceeding 80%, supported by statistically significant quadratic models ($R^2 = 0.9759–0.9878$). The optimized formulation (F13) was subsequently prepared and experimentally validated, exhibiting a particle size of 182.8 ± 44.2 nm, PDI of 0.36 ± 0.01, and zeta potential of +30.1 mV, confirming nanoscale dimensions and electrostatic stability. In vitro release demonstrated sustained kinetics over 24 h, following Korsmeyer–Peppas ($R^2 = 0.9699$, $n = 0.4183$; Fickian diffusion). Ex vivo across excised nasal mucosa, DFP-CSLCNPs achieved higher cumulative permeation (1047.01 vs. 611.46 µg/cm²), greater flux *Jss* (68.18 ± 3.41 vs. 37.22 ± 1.86 µg/cm²·h), and higher *Papp* (68.16 ± 0.36 vs. 37.24 ± 2.12 × 10^{-3} cm/h) than plain solution. Safety evaluations indicated no clinical toxicity over 28 days in Wistar rats.

Conclusion The optimized DFP-CSLCNPs show promise as a safe and effective formulation for intranasal nose to brain targeting of potassium channel blockers for the management of MS.

Keywords Dalfampridine · Nanoparticles · Nose to brain targeting · Multiple sclerosis · Chitosan-lecithin · Safety evaluation

✉ Jose Prakash Dharmian
jose88prakash@gmail.com

[1] Department of Pharmaceutics, Crescent School of Pharmacy, B.S.Abdur Rahman Crescent Institute of Science & Technology, Chennai, Tamil Nadu 600048, India

[2] Sun College of Pharmacy and Research Centre, Kanyakumari District, Tamil Nadu 629204, India

[3] National Institute of Pharmaceutical Education and Research (NIPER)-Kolkata, Chunilal Bhawan, 168, Maniktala Main Road, Kolkata, West Bengal 700054, India

[4] Department of Pharmaceutics, School of Pharmaceutical Sciences, Vels Institute of Sciences, Technology and Advanced Studies, Pallavaram, Chennai, Tamil Nadu 600043, India

Introduction

Multiple Sclerosis (MS) is a long-term, progressive, immune-mediated disease that targets the Central Nervous System (CNS), impacting both the brain and spinal cord. It Characterized by inflammation and demyelination followed by axonal injury. MS causes diverse neurological problems, such as weakness in muscles, persistent fatigue, vision disturbances, cognitive difficulties, and challenges with coordination. The disease affects more than 2.8 million people worldwide, and its prevalence is rising yearly due to better diagnostic approaches and environmental influences.

Published online: 12 April 2026

Although decades of investigation have advanced understanding of MS, its precise pathogenesis remains elusive. Current evidence suggests that genetic predisposition, environmental exposures, notably viral infections and immune system dysregulation collectively contribute to disease onset and progression [1]. One of the most debilitating features of MS is demyelination. Myelin is a fatty substance that protects the nerves and produces efficient electrical impulse transmission. Loss of myelin disrupts communication between neurons, resulting in the clinical manifestations of the disease. Current therapeutic strategies for MS aim to modulate the immune response, reduce the frequency of relapses, delay disease progression, and alleviate specific symptoms. However, many conventional treatments come with limitations, including poor CNS bioavailability, systemic side effects, and the inability to reverse neurodegeneration [2]. DFP is the first medication approved by the FDA. DFP, also known by its chemical name 4-aminopyridine, is a voltage-gated potassium channel blocker that plays a crucial role in improving nerve conduction in demyelinated axons. It is among the few medications specifically approved to enhance walking speed in individuals with MS [3, 4]. It is a small, water-soluble molecule (molecular weight of approximately 94.11 g/mol) with high aqueous solubility because of the presence of a primary amine group, which increases its ionization at physiological pH. Although it has a favorable solubility profile, DFP has a low therapeutic index and dose-dependent adverse reactions, such as seizures, at higher plasma concentrations. The drug is marketed as an oral extended-release tablet (10 mg), usually given twice a day (total daily dose of 20 mg). The drug functions by blocking potassium efflux from demyelinated neurons, thereby prolonging the action potential and enhancing synaptic transmission. Clinically, DFP has been shown to produce modest but significant improvements in motor function and gait in a subset of MS patients [5]. However, DFP presents several pharmacological challenges. Orally administered, it has a short half-life (3–6 h), necessitating frequent dosing, which increases the risk of side effects such as dizziness, insomnia, seizures, and urinary tract infections. Furthermore, the drug has limited ability to permeate the blood-brain barrier (BBB), thereby reducing its effectiveness in targeting pathways specific to the CNS. Such limitations emphasize the importance of developing novel delivery platforms that facilitate precise CNS localization and minimize off-target systemic distribution [6].

The intranasal route offers a promising alternative for delivering therapeutics to the CNS due to its unique anatomical and physiological features. Unlike the oral and intravenous routes, which are limited by first-pass metabolism and restricted drug permeability across the BBB, intranasal administration enables direct nose-to-brain transport via the olfactory and trigeminal neural pathways, thereby improving CNS drug targeting efficiency [7, 8]. The nasal cavity provides a large surface area, rich vascularization, and relatively low enzymatic activity, facilitating rapid and efficient drug absorption. Extensive research indicates that intranasal administration can successfully transport various therapeutic agents, including small molecules, peptides, and nanoparticles, directly to the brain. The non-invasive nature of this route also improves patient compliance, particularly for chronic conditions like MS. However, intranasal administration has its own set of problems, including short residence duration in the nose, enzyme breakdown, and clearance of the mucociliary tract. The challenges associated with conventional delivery can be addressed through the application of nanotechnology-based carriers, which enhance mucoadhesive interaction, preserve the stability of therapeutic molecules against enzymatic degradation, and facilitate regulated, sustained drug release to improve overall delivery efficiency [9]. Nanotechnology has revolutionized drug delivery by enabling the design of carriers that improve solubility, bioavailability, and targeting of therapeutic substances. Increased surface area for interaction with biological tissues, novel and prolonged drug release profiles, protection of encapsulated medications from enzymatic degradation, and the possibility of surface modification to enable targeted delivery are just a few benefits of nanoparticles, which are generally between 1 and 1000 nanometres in size [10]. Polymeric nanoparticles made from biocompatible and biodegradable materials like chitosan and lecithin are particularly useful for intranasal administration because they are non-toxic, FDA-approved, and possess intrinsic properties suitable for mucosal delivery [11, 12]. Lecithin was selected to form a lipid-based nanostructure that provides a diffusional barrier and facilitates interaction with biological membranes, thereby contributing to sustained drug release. Although DFP is hydrophilic, it can still be incorporated within the aqueous domains and at the lipid–water interface of the nanostructure, enabling effective drug accommodation within the carrier system. Chitosan, a naturally derived polysaccharide from chitin, offers excellent mucoadhesive and permeation-enhancing properties, can transiently open tight junctions in epithelial layers of paracellular transport, is biodegradable, and exhibits low immunogenicity, making it ideal for repeated intranasal use. Lecithin, a phospholipid, is another valuable excipient that enhances nanoparticle stability and biocompatibility and facilitates the incorporation of lipophilic drugs. Previous studies have demonstrated the successful use of chitosan and lecithin in nanoparticle formulations for nose-to-brain drug delivery [13].

The rationale for this study is based on the limitations of current DFP formulations and the unmet need

for targeted CNS delivery strategies in MS. A Chitosan-Lecithin nanoparticle system administered via the intranasal route offers a multifaceted solution: it bypasses the BBB, minimizes systemic exposure, provides sustained drug release, and improves patient compliance [14]. Furthermore, prior studies have demonstrated the feasibility of intranasal delivery of neurotherapeutics using similar nanoparticle platforms. However, no comprehensive studies have been reported on the formulation, optimization, and in vivo evaluation of intranasal DFP nanoparticles using a Chitosan-Lecithin matrix [15]. This research primarily aimed to formulate and characterize Chitosan–Lecithin-based DFP nanoparticles for intranasal delivery to improve drug targeting in the CNS for the management of MS. The specific aims included conducting an in-silico study to assess DFP's pharmacodynamic and pharmacokinetic profile and its interaction with CNS targets, performing preformulation studies to assess compatibility between DFP, Chitosan, and Lecithin, formulating nanoparticles using solvent injection approach, and optimizing formulation variables using a Box-Behnken experimental design to achieve desired Particle Size, Zeta Potential, and Encapsulation Efficiency. This work moves the field of CNS drug delivery in MS forward by integrating a biocompatible nanoparticle platform with a non-invasive nose-to-brain delivery strategy. This approach improves the brain bioavailability of DFP, minimizes systemic side effects, and offers controlled drug release. The use of advanced optimization techniques and in vivo assessment ensures scientific validity.

Materials and Methods

Materials

DFP (purified grade) was kindly provided by Hetero Pharmaceuticals Pvt. Ltd., Hyderabad, India. Chitosan (medium molecular weight), lecithin (≥98% phosphatidylcholine), and Poloxamer 407 were procured from Sigma-Aldrich. All other chemicals and reagents used in this study were of analytical grade and were employed without further purification. Ultrapure water was used throughout all experimental procedures.Fresh goat nasal mucosa was obtained from a local registered slaughterhouse through Cape Bio Lab, Marthandam, Tamil Nadu, India, immediately after animal sacrifice. The tissue was transported to the laboratory in cold phosphate buffer solution (pH 6.4) within 1 h of collection and was used for ex vivo permeation studies. Animals were provided with standard pellet feed procured from Krishna Valley Agrotech, Pune, India, and bedding materials supplied by Cape Bio Lab and Research Centre, Marthandam, Tamil Nadu, India.

In Silico Evaluation of DFP

The crystal structures of MSBI1.176 WH1 domain (replication protein derived from a MS patient; PDB ID: 6H24), RNA G2C4 repeats in both native form (PDB ID: 8QMI) and complex with the synthetic ligand ANP77 (PDB ID: 8QMH), human WDR5 associated with PTEN (PDB ID: 8 × 3 S), and human tyrosine–protein kinase C-SRC (PDB ID: 1FMK) were obtained from the RCSB Protein Data Bank (www.rcsb.org). Only structures with a resolution below 3 Å were considered, and all were downloaded in PDB format for further analysis. The ligand DFP was downloaded from the PubChem database in SDF format. Binding affinity prediction was performed using PyRx software. Since PyRx requires the receptor and ligand in PDB format, the ligand was converted from SDF to PDB format using Open Babel GUI software. Both the receptor and ligand were imported into PyRx software. A grid box was developed, and the binding affinity was predicted. Protein-ligand interactions were analyzed using Biovia Discovery Studio 2021. The protein and ligand were imported, defined, and interactions were visualized by clicking "Ligand Interaction." The resulting 3D and 2D interaction images were saved as image files. Protein interactions were then predicted using the 2D interaction image. The Swiss ADME portal was utilized for the ADMET study of the selected ligand. By pasting the ligand's SMILES notation into the portal and clicking "Run," the ADMET report was generated. Additionally, Ramachandran plot analysis was performed for structural validation, the BOILED-Egg model was used to predict BBB permeability, and hydrophobicity assessments were conducted to characterize the compound's physicochemical properties. The in silico analysis was not conducted to reconfirm the established pharmacological activity of DFP, but rather to explore its potential molecular interactions with neuronal targets associated with demyelination and to provide mechanistic insight supporting the rationale for intranasal brain-targeted delivery.

Preparation of DFP-CSLCNP

The DFP-CSLCNP formulation was prepared using the solvent injection technique. In this method, 5 mg of DFP and lecithin (LC) were dissolved in approximately 1–5 mL of ethanol to form an ethanolic mixture of DFP and LC, as shown in Fig. 1 [16]. A glacial acetic acid-prepared aqueous acidic solution was used to dissolve Chitosan (CS) and Poloxamer 407. Poloxamer was incorporated as a steric stabilizer to prevent particle aggregation, reduce polydispersity, and enhance overall colloidal stability. Chitosan was included to confer a positive surface charge and improve mucoadhesive properties, thereby prolonging

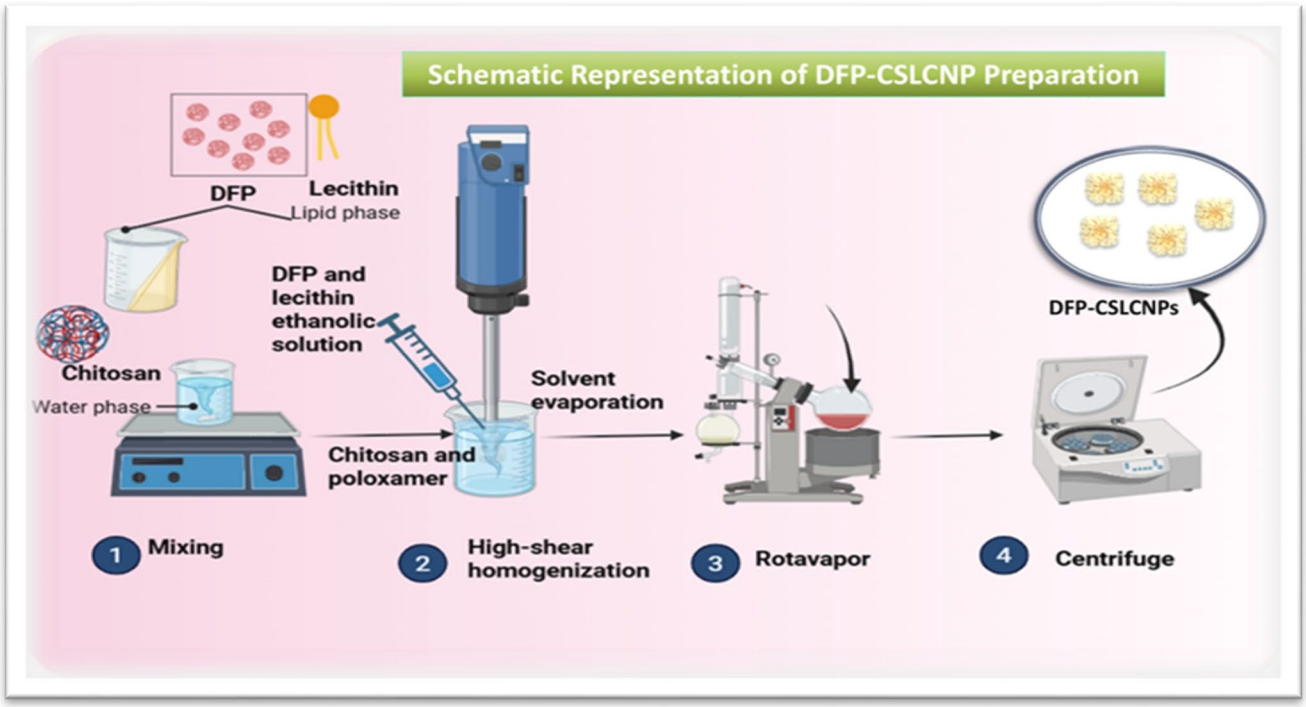

Fig. 1 A schematic representation of the preparation of DFP-loaded Chitosan Lecithin Nanoparticle (DFP-CSLCNPs) by the solvent injection method

nasal residence time and potentially enhancing paracellular transport through transient modulation of tight junctions. An ethanolic solution was injected into the aqueous phase using a polypropylene syringe fitted with a 22G needle. The process was performed under high-speed homogenization (12,000 rpm) for five minutes. The organic solvent from the resulting nano-dispersion was removed using a Rotavapor for ten minutes. Following solvent removal, the dispersion was centrifuged for 1 h at 45,000 rpm at 4 °C to obtain the DFP-CSLCNP pellet. After carefully discarding the supernatant, the pellet was collected for further use [17–20]. In addition, DFP-CSLCNP pellets were cleaned three times using Milli-Q water to get rid of any remaining free drug residue. For lyophilisation, the final pellet of DFP-loaded Chitosan–Lecithin Nanoparticles (DFP-CSLCNPs) were re-dispersed in a 10% w/v mannitol solution, with mannitol serving as a cryoprotectant. The prepared dispersion was freeze-dried, and the resulting lyophilized DFP-CSLCNPs powder was stored at refrigerated conditions (2–8 °C) until further use [21].

Experimental Design

Optimization of DFP-loaded Chitosan–Lecithin Nanoparticles (DFP-CSLCNPs) was carried out through a Box–Behnken response surface design involving three key factors. The design was generated and analyzed using Design Expert® software (version 23.1.8.0, Stat-Ease Inc., Minneapolis, MN, USA). Three formulation factors, namely Chitosan, Lecithin, and Poloxamer 407 concentrations, were used as independent variables and assessed at three coded levels (− 1, 0, + 1). The design was structured to assess their influence on the critical dependent responses, including Particle Size, Zeta Potential, and Entrapment Efficiency of DFP-CSLCNPs. The suitability of the model was verified through ANOVA analysis, and optimization was achieved by selecting conditions that produced the smallest particle size, highest drug entrapment, and consistent zeta potential. The finalized formulation was then subjected to comprehensive physicochemical and biological assessments [22].

The ranges of formulation variables explored through the Box–Behnken design are listed in Table 1, with factors coded at three levels (–1, 0, and + 1). The amounts of Chitosan (A), Poloxamer 407 (B), and Lecithin (C) were chosen as the

Table 1 Experimental levels of independent variables in Box-Behnken design for DFP- CSLCNPs optimization

Independent Variables	Levels		
	-1	0	+1
Chitosan (mg)	0.5	2.75	5
Poloxamer 407 (mg)	0.5	5.25	10
Lecithin (mg)	20	59	98

-1 represents low level, 0 represents center point, + 1 represents high level

independent variables based on their significant influence on the formulation process. The dependent responses selected for the study were particle size (Y_1), zeta potential (Y_2), and entrapment efficiency (Y_3). According to the Box–Behnken Design, a total of seventeen formulations, including five center points, were developed. For each DFP-CSLCNPs formulation, the response variables, including particle size, zeta potential, and entrapment efficiency (%EE), were systematically determined. All measurements were carried out in triplicate, and the data are reported as mean values with standard deviation (mean ± SD). The adequacy of the model was evaluated using statistical parameters, with a particular emphasis on achieving higher R^2 values. The equations obtained from Design-Expert® software were employed to generate 2D contour and 3D response surface plots, enabling visualization of the relationships between the independent and response variables. A three-factor, seventeen-run Box-Behnken design was used in the present investigation, and this design was employed to study the effect of formulation variables, including chitosan (A), poloxamer 407 (B), and lecithin (C), on the particle size (Y_1), zeta potential (Y_2), and entrapment efficiency (Y_3) of DFP-loaded chitosan-lecithin nanoparticles (DFP-CSLCNPs). The independent variables were evaluated at different levels, and the corresponding response values obtained showed significant variation in all three dependent responses. Particle size ranged from 18 to 170 nm, zeta potential varied between 8 and 49 mV, and entrapment efficiency was found to be between 20% and 90% for different runs. This experiment proves that by altering the concentration of chitosan, poloxamer 407, and lecithin, the responses are highly variable, indicating a strong influence of formulation composition on the characteristics of nanoparticles. Thus, the design clearly demonstrates that the responses are dependent and significantly affected by the selected formulation parameters, helping in understanding and prediction of optimum levels required to achieve desirable DFP-CSLCNP characteristics.

Particle Size and Surface Charge (Zeta Potential)

Particle size and polydispersity index (PDI) were determined by Dynamic Light Scattering (DLS), while Zeta Potential was evaluated through Electrophoretic Light Scattering (ELS) using a HORIBA SZ-100 Nanoparticle Analyzer (Model SZ-100V2, HORIBA Scientific, Kyoto, Japan). Measurements were conducted with SZ-100 software (version 2.42) at a controlled temperature of 25 ± 1 °C. Samples were suitably diluted with deionized water to minimize multiple scattering effects. Each analysis was carried out in triplicate, and results are presented as mean ± standard deviation (SD).

Scanning Electron Microscopy (SEM)

The surface character and size of DFP-CSLCNPs were evaluated by SEM (ZEISS EVO 18, Carl Zeiss, Germany). Samples were centrifuged, washed, dried, mounted on aluminium stubs, sputter-coated with gold, and imaged under high vacuum at 5–10 kV. Particle dimensions were determined from ≥100 measurements using SmartSEM software, and data are expressed as mean ± SD.

Transmission Electron Microscopy (TEM)

The morphology and internal structure of DFP-CSLCNPs were analysed using TEM (Thermo Scientific™ Talos F200C, USA) operated at 120–200 kV in bright-field mode. Diluted and sonicated samples were placed on glow-discharged carbon-coated copper grids, air-dried, and imaged with a Ceta 4k × 4k CMOS camera. Particle dimensions were determined from ≥150 measurements using Velox software and compared with DLS data.

Entrapment Efficiency

The amount of DFP ($W_{Free\ DFP}$) that was not entrapped was used to calculate the entrapment efficiency (%EE). The DFP suspension was isolated from the free DFP by centrifuging it for one hour at 5,000 rpm. The proven UV-visible spectroscopy analytical method at λmax 262 nm was used to detect free DFP ($W_{Free\ DFP}$) in the supernatant. Entrapment efficiency (%EE) of DFP-CSLCNPs was estimated using the equation below

$$\%EE = \left(\frac{W\ Total\ DFP - W\ Free\ DFP}{W\ Total\ DFP}\right) * 100$$

$W_{Free\ DFP}$ is the unentrapped DFP, and W_{Total} DFP is the entire amount of DFP needed to create DFP- CSLCNP.

Release Kinetics of DFP from CSLCNPs

The in vitro release profile of DFP from the optimized DFP-CSLCNPs and plain drug solution (DFP-SOLN) was evaluated using the dialysis bag diffusion method (molecular weight cut-off: 12–14 kDa, Spectra®, USA). A 2 mL aliquot of each formulation, equivalent to 1 mg of DFP, was loaded into pre-soaked dialysis membranes, securely sealed, and immersed in 500 mL of phosphate buffer (pH 7.4) containing 5% ethanol. The addition of ethanol was not to enhance solubility, but to help maintain consistent sink conditions and reduce potential drug adsorption to the dialysis membrane during the prolonged release study.

The large dissolution volume ensured that the drug concentration remained well below saturation throughout the experiment. The setup was maintained at 37 ± 0.5 °C under continuous stirring at 100 rpm. At predetermined intervals over 24 h, 5 mL of the release medium was withdrawn and replaced with an equal volume of fresh buffer to maintain sink conditions. The concentration of DFP in the collected samples was determined using UV–Vis spectrophotometry at 262 nm following appropriate dilution. Drug release data were analyzed according to zero-order, first-order, Higuchi, Korsmeyer–Peppas, and Hixson–Crowell kinetic models, with correlation coefficients (R^2) used to determine the best-fitting model. The diffusion exponent (n) from the Korsmeyer–Peppas equation was employed to elucidate the release mechanism, where $n \leq 0.45$ indicates Fickian diffusion. All model fitting and kinetic calculations were performed using Microsoft Excel.

Ex Vivo Nasal Drug Permeation

The nasal mucosa of a goat's nose was obtained from a nearby slaughterhouse. With a diffusion area of 0.785 cm^2, the Franz diffusion cell (Orchid Scientific, Nasik, India) was employed. A 1 mL aliquot of the developed formulation, equivalent to 1 mg of DFP, was placed in the donor compartment of the Franz diffusion cell (effective diffusion area: 0.785 cm^2). The receptor compartment was filled with 5 mL of phosphate-buffered saline (PBS, pH 6.4) and maintained at 33 ± 1 °C to simulate nasal physiological conditions. After lyophilization, the nanoparticles were reconstituted with 1 mL of distilled water to restore the original dispersion concentration prior to experimentation. Samples were centrifuged at 15,000 rpm for 15 min at 4 °C using an Eppendorf® centrifuge (Hamburg, Germany) to separate residual nanoparticulate matter from the permeated drug before RP-HPLC analysis, thereby ensuring accurate quantification of the free drug.

Naso Ciliotoxicity and Biocompatibility of DFP -CSLCNPs

Freshly excised goat nasal mucosa was used to perform an 8-h nasal ciliotoxicity study. Untreated mucosa acted as the negative control, whereas tissues treated with DFP-CSLCNPs for 8 h comprised the test group. During the experiment, care was taken to preserve the viability of the nasal membrane. After treatment, the tissues were fixed in 10% neutral-buffered formalin, processed for paraffin embedding, sectioned, and stained with Haematoxylin and Eosin (H&E). Histopathological examination under a light microscope was performed to evaluate tissue architecture and identify any evidence of ciliotoxicity or pathological changes, thereby confirming the biocompatibility and safety of the formulation [23].

Stability Study of DFP-CSLCNPs

Accelerated stability studies were conducted over a 45-day period under controlled environmental conditions of 40 ± 2 °C and 75 ± 5% relative humidity (RH), in accordance with ICH guidelines. The nanoparticle formulations were stored in airtight amber glass vials and examined at predetermined intervals (0, 7, 14, and 45 days) to assess particle size, zeta potential, drug content, and physical appearance.

Toxicological Assessment of DFP-CSLCNPs Formulation

To assess the safety profile of the optimized DFP-CSLCNPs formulation, a 28-day sub-acute toxicity study was conducted using male Wistar rats (2–3 months old, 150–250 g), depicted in Fig. 2. The study protocol complied with the guidelines of the Committee for Control and Supervision of Experiments on Animals (CPCSEA) and was approved by the Institutional Animal Ethics Committee of Cape Bio Lab and Research Centre, Tamil Nadu, India (approval no. CBLRC/IAEC/03/01-2025). Animals were randomly allocated into four groups ($n = 6$ each): a control group treated with vehicle alone, and three test groups receiving intranasal DFP-CSLCNPs at doses of 1, 2, and 4 mg/kg body weight, respectively. Animals were anesthetized with ether before intranasal administration, which was carried out using a polyethylene cannula (10–15 mm insertion) attached to a calibrated micropipette (Eppendorf India Ltd).

Under standardized laboratory conditions, animals were kept at 22 ± 2 °C with 55 ± 5% Relative Humidity and a 12-hour light/dark cycle, with continuous access to food (standard pellet diet) and water [24]. During the 28-day study period, the rats were closely observed for any pathological alterations, such as nasal discharge, bleeding, twitching, irritation of the nostrils, excessive blinking, ocular discomfort, erythema, or unusual behavioural movements both inside and outside the cage before and after intranasal dosing. Systemic toxicity and mortality were evaluated through direct visual inspection, and any abnormal clinical signs were documented. Animals were monitored daily for clinical signs, body weight changes, and food intake [25].

On days 14 and 28, blood samples were collected from anesthetized animals following intraperitoneal administration of ketamine (75 mg/kg) and xylazine (5 mg/kg). The samples were drawn from the retro-orbital plexus using EDTA-coated tubes to prevent coagulation. Samples were centrifuged at 10,000 rpm for 20 min at 4 °C, and the obtained serum was refrigerated until biochemical analysis.

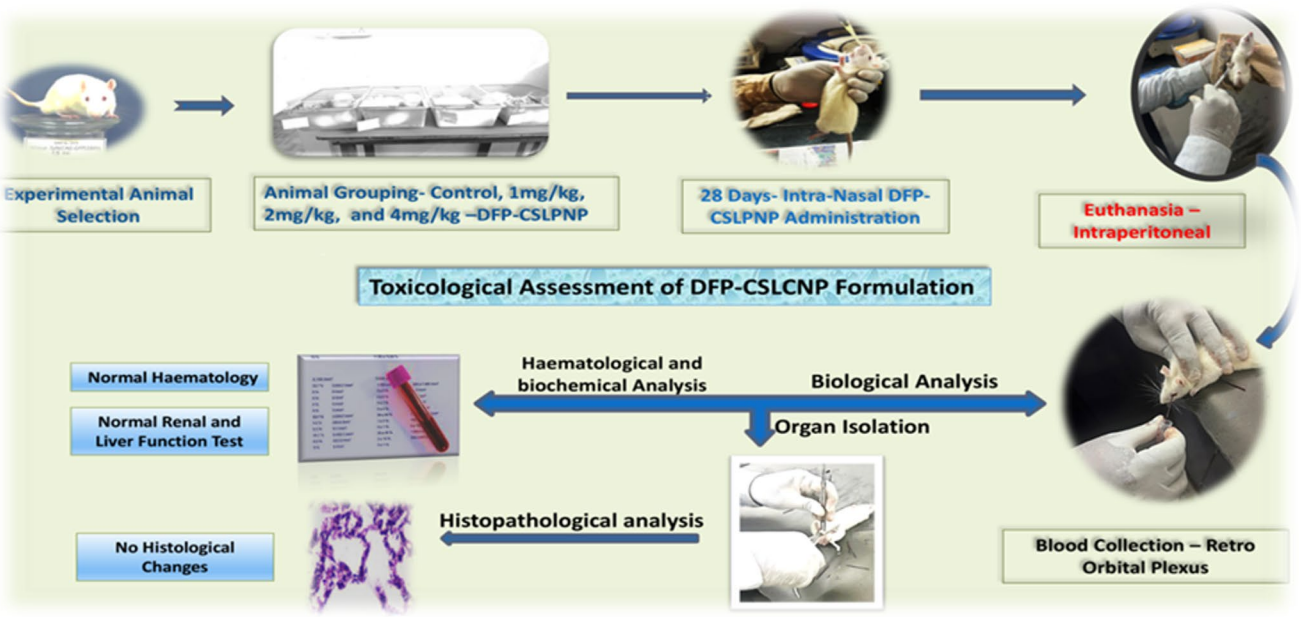

Fig. 2 A schematic representation of the toxicological assessment of DFP-loaded Chitosan Lecithin Nanoparticle (DFP-CSLCNPs)

Serum was assessed for liver function markers (AST, ALT, ALP, Direct Bilirubin, and glucose), kidney function indices (Urea and Creatinine), and lipid profile parameters (Cholesterol, Triglycerides, VLDL) using commercial diagnostic kits. Hematological parameters, including hematocrit, total WBC, Lymphocytes, Polymorphs, Eosinophils, RBC count, platelet count, Mean Cell Volume, Mean Cell Hemoglobin, Hemoglobin, and Mean Erythrocyte Volume, were also evaluated [26].

Immediately after sacrifice, the major organs (Brain, Liver, Kidney, Spleen, Heart, Lungs, and Pancreas) were carefully dissected, rinsed with sterile Phosphate-Buffered Saline (PBS) to remove residual blood, and weighed using an analytical balance. Both absolute and relative organ weights were recorded prior to histopathological evaluation. The excised tissues were trimmed into small sections and fixed in 10% neutral-buffered formalin. Standard histopathological procedures were followed, including dehydration in graded isopropyl alcohol, clearing in xylene, and paraffin embedding for approximately 2 h. Paraffin-embedded L-shaped blocks were prepared, and thin tissue sections were obtained using a rotary microtome. The sections were stained with Haematoxylin and Eosin (H&E) and examined under a light microscope equipped with a digital imaging system to evaluate structural and cellular alterations [23, 27].

Statistical Analysis

All quantitative evaluations, including particle size, zeta potential, and encapsulation efficiency, were conducted in triplicate, and the results are presented as mean ± standard deviation (SD). Statistical analyses were carried out using GraphPad Prism software (version 10.4.2). Comparisons between the control and treatment groups were made using one-way analysis of variance (ANOVA) followed by Dunnett's post hoc test, with a p-value ≤ 0.05 considered statistically significant.

Results and Discussion

In Silico Evaluation of DFP

The docking results of DFP with various protein targets reveal significant insights into its potential as a therapeutic agent for MS. The 6H24 receptor, which represents the WH1 domain associated with MS, showed the maximum interaction strength with DFP, recording a docking energy of −11.2 kcal/mol, as detailed in Table 2. This strong interaction, mediated by critical amino acids such as Isoleucine (ILE), Asparagine (ASN), Proline (PRO),

Table 2 Binding affinity values (kcal/mol) and interacting amino acid residues are listed for each protein–ligand DFP complex

Proteins	Ligand	Binding affinity (Kcal/mol)	Amino acid interaction
6H24	DFP	-11.2	ILE, ASN, PRO, ASP, HOH
8QMI	DFP	-8.2	-
8QMH	DFP	-7.7	HOH
8 × 3 S	DFP	-7.2	LYS, SER, HIS, HOH
1FMK	DFP	-7.6	LEU, ALA, SER

Aspartic acid (ASP), and water molecules (HOH), suggests that this protein could be a relevant target in modulating MS-related pathways. The WH1 domain plays a key role in signal transduction and cellular regulation, and its interaction with a high-affinity ligand such as DFP could potentially modulate neural signaling and immune activity, thereby influencing disease progression in MS. The other protein targets—8QMI (RNA G2C4 repeats), 8QMH (RNA G2C4 complexed with ANP77), 8 × 3 S (WDR5 complexed with PTEN), and 1FMK (human tyrosine-protein kinase C-SRC)—showed comparatively lower binding energies. However, these results still indicate that DFP establishes stable and favorable interactions with these proteins, as presented in Fig. 3. These proteins play roles in cellular processes such as RNA regulation, epigenetic modifications, and kinase signaling, all of which are potentially implicated in the inflammatory and neurodegenerative aspects of MS. The high binding affinity of DFP to 6H24, a protein relevant to MS, aligns with its known clinical use as a symptomatic treatment for the disease, where it improves walking ability in patients by blocking potassium channels in demyelinated neurons, restoring neural conduction. This molecular docking analysis further supports the idea that DFP may exert broader effects on MS through interactions with multiple proteins involved in neurological and immunological functions. Further research is warranted to explore these interactions at the cellular level, which could open new avenues for therapeutic interventions in MS beyond symptomatic relief, potentially addressing the disease's underlying pathology.

The Swiss ADME analysis of DFP provides significant insights into its suitability as a therapeutic agent, particularly for neurological conditions like MS. DFP is a small, rigid molecule with a molecular weight of 94.11 g/mol and no rotatable bonds, indicating a stable structure. The compound exhibits moderate polarity, as evidenced by a TPSA of 38.91 Å², which favors its transmembrane permeability and thereby supports its potential to exert CNS activity, as illustrated in Fig. 4a.With a consensus log P of 0.47, the compound demonstrates moderate lipophilicity, which supports its ability to penetrate the BBB—a critical requirement for agents developed to act on the CNS. Additionally, DFP shows high water solubility across multiple solubility models, which enhances its oral bioavailability and systemic absorption. The pharmacokinetics profile is particularly favorable, as DFP demonstrates high gastrointestinal (GI) absorption and the ability to cross the BBB. Notably, it is not a substrate for P-glycoprotein (P-gp), reducing the risk of efflux out of the brain, which could otherwise limit its efficacy. Notably, the compound shows no inhibitory effect on key cytochrome P450 isoenzymes (CYP1A2, CYP2C19, CYP2C9, CYP2D6, and CYP3A4), which reduces the risk of metabolic drug–drug interactions and enhances its suitability for patients receiving combination therapies.

DFP satisfies all criteria of Lipinski's Rule of Five without any violations, indicating favorable properties for

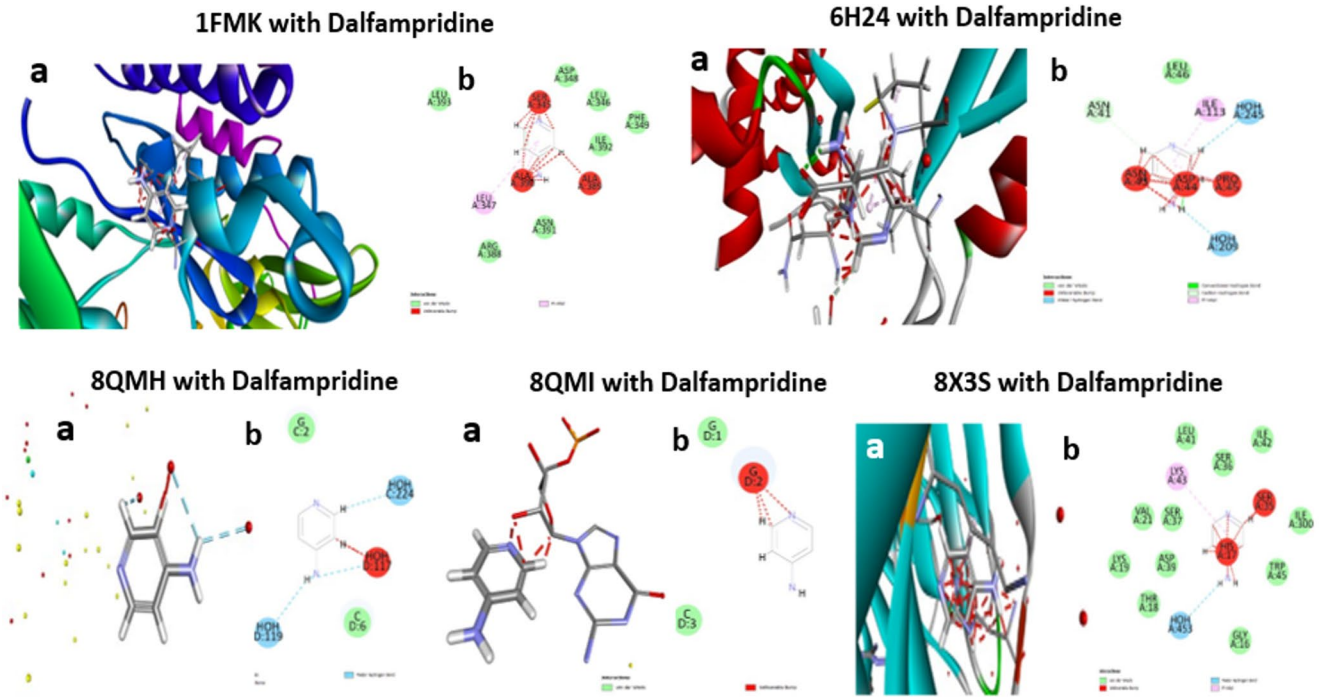

Fig. 3 Molecular docking 3D poses (**a**) and 2D interaction (**b**) diagrams of Ligand DFP with CNS-relevant Potassium Channel protein targets. (green for hydrophobic contacts, red for hydrogen bond acceptors, blue for hydrogen bond donors, and purple for other interactions)

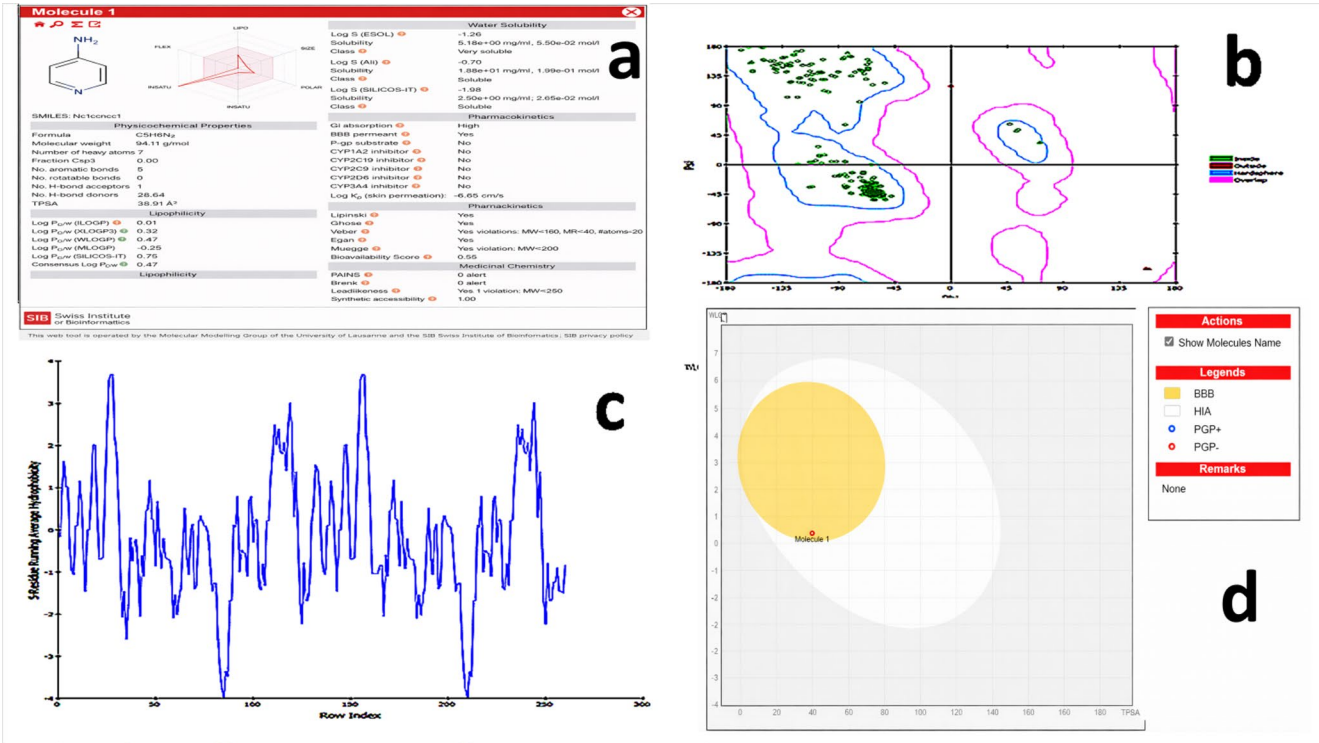

Fig. 4 **a**. ADMET profile of (**b**) Ramachandran plot, (**c**) Molecular hydrophobicity surface plot, (**d**) Swiss Boiled Egg model of DFP

development as an orally active drug. However, it does have some Ghose filter violations due to its small size and molecular refractivity, which are not uncommon in highly potent CNS-active drugs. The compound has a bioavailability score of 0.55, further reinforcing its potential for efficient oral dosing. Additionally, the absence of PAINS or Brenk alerts highlights the absence of problematic functional groups, while its synthetic accessibility score of 1.00 suggests ease of chemical synthesis. In summary, DFP's physicochemical and pharmacokinetic properties, along with its compliance with most drug-likeness filters, support its effectiveness as an oral drug for managing MS. Its ability to cross the BBB, combined with high solubility and minimal risk of drug interactions, positions it as a well-suited candidate for targeting neurological symptoms in patients with MS [28–31].

The Ramachandran plot of the X-ray crystal structure of the MSBI1.176 WH1 domain (PDB ID: 6H24), a replication-associated protein identified in a MS patient, illustrates the distribution of backbone dihedral angles (Φ and Ψ) for individual residues. The majority of the residues are situated within the most favorable regions, represented by green dots, indicating that these residues adopt stable conformations typically found in alpha-helices and beta-sheets. The blue contour regions correspond to residues in allowed conformations, which are slightly less energetically favorable but still free from steric clashes. Meanwhile, the pink contour lines denote regions with potential steric overlap, suggesting less favorable or strained backbone conformations. The few red dots and triangles indicate outliers that fall into disallowed regions of the plot. These residues might be located in flexible or loop regions of the protein, where unusual dihedral angles are more common, or could be crystallographic artifacts. Overall, the plot demonstrates a well-folded protein structure, with the majority of residues conforming to expected secondary structural elements. The presence of a small number of outliers warrants further investigation to confirm whether these are biologically relevant or due to structural refinement issues. The plot indicates that the protein adopts a characteristic fold typical of replication-associated proteins, aligning with its proposed function in DNA binding, as shown in Fig. 4b.

The hydrophobicity plot for the X-ray crystal structure of the MSBI1.176 WH1 domain (PDB ID: 6H24) illustrates the variation in hydrophobicity along the sequence of the replication protein. The plot is based on a 5-residue running average of hydrophobicity, which smooths out fluctuations to reveal patterns in hydrophobicity across the protein. Figure 4c, in this plot, regions with higher hydrophobicity (positive values) are likely to be involved in forming the protein's hydrophobic core, crucial for maintaining the structural stability of the folded domain. These hydrophobic stretches may be buried within the protein or interacting with other hydrophobic regions, contributing to the compact

and stable tertiary structure. On the other hand, regions with lower or negative hydrophobicity values correspond to hydrophilic residues, which are more likely to be exposed to the solvent and contribute to interactions with water or other polar molecules. The fluctuations between hydrophobic and hydrophilic regions suggest a typical pattern for globular proteins, where hydrophobic residues are sequestered in the interior, and hydrophilic residues are located on the surface. Peaks in the positive hydrophobicity regions might represent sections involved in secondary structure elements like alpha-helices or beta-sheets, contributing to the protein's functional domains. Meanwhile, troughs in the plot, particularly those that dip below zero, may correspond to flexible loop regions or areas with polar or charged residues that are solvent-exposed. This hydrophobicity profile provides insights into the structural arrangement of the protein, indicating how hydrophobic and hydrophilic residues are distributed to form a stable and functional domain [32–34]. In Fig. 4d, the swissBOILED-Egg model shows that DFP lies within the BBB-permeant region, indicating strong potential for brain penetration. With a TPSA of 38.91 Å² and WLOGP of ~ 1.2, DFP exhibits moderate polarity and optimal lipophilicity, favoring membrane permeability. Its PGP– classification suggests it is not a substrate for efflux transporters, further supporting its suitability for CNS delivery and therapeutic action in MS.

Optimization of DFP-CSLCNPs Using Box–Behnken Design

To optimize the formulation, a three-factor, three-level Box–Behnken design was adopted, enabling the assessment of interactions between independent formulation variables and their impact on dependent responses for DFP-loaded Lecithin–Chitosan nanoparticles.

The general form of the quadratic polynomial model used for optimization is given by:

$$Y = {}_0 + {}_1A + {}_2B + {}_3C + {}_{12}AB + {}_{13}AC + {}_{23}BC + {}_{11}A^2 + {}_{22}B^2 + {}_{33}C^2$$

In the developed quadratic model, Y denotes the measured response variable, such as particle size, zeta potential, or entrapment efficiency. The constant term β_0 represents the intercept, while β_1, β_2, and β_3 correspond to the linear effects of the independent variables. The interaction effects between the factors are expressed by β_{12}, β_{13}, and β_{23}, and the curvature or quadratic effects are defined by β_{11}, β_{22}, and β_{33}. Here, A, B, and C represent the concentrations of chitosan, poloxamer 407, and lecithin, respectively. This model structure enables the evaluation of both individual and interactive influences of formulation variables on the desired nanoparticle characteristics.

The outcomes of the ANOVA test validated the robustness of the quadratic model in explaining variations in Particle Size, Zeta Potential, and Entrapment Efficiency, as evidenced by highly significant p-values (<0.0001) across all three responses. Table 3 shows the R^2 values, which were 0.9759 for Particle Size, 0.9878 for Zeta Potential, and 0.9820 for Entrapment Efficiency, indicating a good fit of the model to the experimental data. The adjusted R^2 values (0.9449 for Particle Size, 0.9721 for Zeta Potential, and 0.9588 for Entrapment Efficiency) and predicted R^2 values (0.8744 for Particle Size, 0.8666 for Zeta Potential, and 0.9222 for Entrapment Efficiency) were in reasonable agreement, suggesting the model's predictive capability. The model demonstrated strong statistical validity, as reflected by Adequate Precision values of 17.7152, 23.8378, and 21.9565 for Particle Size, Zeta Potential, and Entrapment Efficiency, respectively. These values, being far higher than the minimum requirement, indicate an excellent signal-to-noise ratio and confirm that the model is capable of effectively guiding optimization within the design space.

Table 4 represents the model F-values of 31.51 for particle size, 62.95 for zeta potential, and 42.37 for entrapment efficiency, further confirming their significance. Furthermore, the lack of fit p-values (0.2133 for Particle Size, 0.6216 for Zeta Potential, and 0.9902 for entrapment efficiency) being greater than 0.05 indicated that the lack of fit was not significant, which is desirable for a well-fitting model.

Table 3 Best-Fitting Model for the Dependent Responses: Particle Size, Zeta Potential, and Entrapment Efficiency of DFP-CSLCNPs

Response	Model	*R*-Squared (r2)	Adjusted r2	Predicted r2	Std. Dev	%CV	Adequate Precision	Remarks
Particle size (nm)	Linear	0.1498	-0.0464	-0.5393	50.77	-	-	-
	2FI	0.2248	-0.2403	-5.5794	55.27	-	-	-
	Quadratic	**0.9759**	**0.9449**	**0.8744**	**11.65**	**13.07**	**17.7152**	**Suggested**
Zeta potential (mV)	Linear	0.2014	0.0171	-0.4896	13.15	-	-	-
	2FI	0.2357	-0.2229	-9.0226	14.67	-	-	-
	Quadratic	**0.9878**	**0.9721**	**0.8666**	**2.22**	**7.88**	**23.8378**	**Suggested**
Entrapment Efficiency (%EE)	Linear	0.1078	-0.0981	-0.6286	21.47	-	-	-
	2FI	0.3657	-0.0149	-2.7473	20.64	-	-	-
	Quadratic	**0.9820**	**0.9588**	**0.9222**	**4.16**	**7.15**	**21.9565**	**Suggested**

Table 4 Data fitting and model selection using Box–Behnken design

Source	Sum of Squares	df	Mean Square	F-value	*p*-value	
Particle size -Y_1 (nm)						
Model- Quadratic	**38464.41**	**9**	**4273.82**	**31.51**	**<0.0001**	**Significant**
A-Chitosan	20837.37	1	20837.37	153.64	<0.0001	
B-Poloxamer 407	5727.19	1	5727.19	42.23	0.0003	
C-Lecithin	717.46	1	717.46	5.29	0.0550	
AB	3821.17	1	3821.17	28.18	0.0011	
AC	584.00	1	584.00	4.31	0.0766	
BC	2583.93	1	2583.93	19.05	0.0033	
A^2	21456.11	1	21456.11	158.20	<0.0001	
B^2	1790.29	1	1790.29	13.20	0.0084	
C^2	147.08	1	147.08	1.08	0.3323	
Residual	949.36	7	135.62			
Lack of Fit	**936.86**	**6**	**156.14**	**12.49**	**0.2133**	**Not Significant**
Pure Error	12.50	1	12.50			
Cor Total	39413.76	16	-			
Zeta potential- Y_2 (mV)						
Model- Quadratic	**2781.40**	**9**	**309.04**	**62.95**	**<0.0001**	**Significant**
A-Chitosan	876.18	1	876.18	178.46	<0.0001	
B-Polaxamer 407	897.81	1	897.81	182.87	<0.0001	
C-Lecithin	285.11	1	285.11	58.07	0.0001	
AB	10.63	1	10.63	2.16	0.1847	
AC	522.67	1	522.67	106.46	<0.0001	
BC	13.36	1	13.36	2.72	0.1430	
A^2	1172.33	1	1172.33	238.78	<0.0001	
B^2	558.25	1	558.25	113.71	<0.0001	
C^2	455.48	1	455.48	92.77	<0.0001	
Residual	34.37	7	4.91			
Lack of Fit	**29.87**	**6**	**4.98**	**1.11**	**0.6216**	**Not Significant**
Pure Error	4.50	1	4.50			
Cor Total	2815.76	16				
Entrapment Efficiency-Y_3 (%EE)						
Source	**Sum of Squares**	**df**	**Mean Square**	**F-value**	**p-value**	
Model Quadratic	**6592.74**	**9**	**732.53**	**42.37**	**<0.0001**	**Significant**
A-Chitosan	362.27	1	362.27	20.95	0.0026	
B-Polaxamer 407	480.68	1	480.68	27.80	0.0012	
C-Lecithin	369.39	1	369.39	21.37	0.0024	
AB	813.38	1	813.38	47.05	0.0002	
AC	48.45	1	48.45	2.80	0.1381	
BC	572.63	1	572.63	33.12	0.0007	
A^2	386.76	1	386.76	22.37	0.0021	
B^2	1113.50	1	1113.50	64.41	<0.0001	
C^2	1125.83	1	1125.83	65.12	<0.0001	
Residual	121.02	7	17.29			
Lack of Fit	**36.52**	**6**	**6.09**	**0.0720**	**0.9902**	**Not Significant**
Pure Error	84.50	1	84.50			
Cor Total	6713.76	16				

Impact of Independent Variables and their Interactions on Response Parameters

The Box–Behnken design analysis indicated that the quadratic model was the most appropriate for interpreting the experimental outcomes, with the derived polynomial equations demonstrating the effects of formulation parameters on particle size (Y1), zeta potential (Y2), and entrapment efficiency (Y3).

Factor A demonstrated a positive effect on response Y1, while factors B and C exerted negative effects on Y1 in the DFP-CSLCNPs formulation. The combined interactions of A with B resulted in a negative impact on Y1. In contrast,

the interaction between A with C and B with C showed a positive influence on this response.

$$\mathbf{Y}_1 = 45.72 + 142.41\mathrm{A} - 66.53\mathrm{B} - 13.81\mathrm{C} - 10.57\mathrm{AB} + 5.33\mathrm{AC} + 9.28\mathrm{BC} - 31.54\,\mathrm{A}^2 + 12.36\mathrm{B}^2 + 7.34\,\mathrm{C}^2$$

$$\mathbf{Y}_2 = 26.06 + 29.20\mathrm{A} - 26.34\mathrm{B} + 8.71\mathrm{C} + 0.5576\mathrm{AB} + 5.04\mathrm{AC} - 0.6672\mathrm{BC} - 7.37\mathrm{A}^2 + 6.90\mathrm{B}^2 - 12.91\mathrm{C}^2$$

In the optimization of DFP-CSLCNPs, response Y2 was positively influenced by both factors A and C, while factor B had an adverse impact. Synergistic interactions of A with B and A with C influenced Y2, but the B & C combination negatively affected the response.

$$\mathbf{Y}_3 = 53.33 + 18.78\mathrm{A} + 19.27\mathrm{B} - 9.91\mathrm{C} - 4.88\mathrm{AB} - 1.53\mathrm{AC} - 4.37\mathrm{BC} - 4.23\mathrm{A}^2 - 9.75\mathrm{B}^2 + 20.30\mathrm{C}^2$$

For the DFP-CSLCNPs, factors A and B demonstrated a positive effect on response Y3, whereas factor C exerted an adverse influence. The combined interactions of A with B, A with C, and B with C all negatively affected Y3. The influence of the independent formulation variables chitosan concentration, Poloxamer 407 concentration, and Lecithin concentration on Particle Size, Zeta Potential, and Entrapment Efficiency is depicted in Figs. 5 and 6 through Three-Dimensional response surface plots and Two-Dimensional contour plots.

Applied Model Validation of the Optimized Formulation

The optimized DFP-CSLCNPs formulation (F13) displayed a mean particle size of 182.8 ± 44.2 nm with a polydispersity index (PDI) of 0.36 ± 0.01, as illustrated in Fig. 7a. The low PDI value reflects a narrow and homogeneous particle size distribution, which ensures uniform drug release from the nanoparticles. The nanoscale dimension of the formulation provides a larger surface area-to-volume ratio, facilitating improved drug diffusion and absorption through the intranasal (i.n.) route. Figure 7b revealed that the zeta potential was measured at approximately + 30.1 mV and the Electrophoretic Mobility Mean 0.000233 cm2/Vs, signifying adequate electrostatic stability and the mucoadhesive potential of chitosan-coated particles. The positive surface charge is advantageous for nasal delivery due to enhanced interaction with negatively charged mucosal surfaces. Entrapment efficiency ranged from 40.2 ± 1.8% to 82.3 ± 0.5% depending on formulation ratios, with the optimized batch showing the highest efficiency. The experimentally observed values for the dependent variables of the optimized DFP-CSLCNPs formulation closely matched the predicted values, demonstrating the accuracy and reliability of the applied statistical model. Wide consensus has been found between the optimization behavior seen in this study and previously documented lecithin–chitosan nanoparticle systems, especially the work of Walbi IA et al. 2022. Second-order polynomial equations are suitable for characterizing the nonlinear connections regulating lecithin–chitosan nanoparticle systems, as indicated by the good statistical reliability of the quadratic model produced via Box–Behnken design in both studies. The predominance of chitosan concentration as the primary factor controlling nanoparticle properties is a significant commonality. Regarding drug entrapment, our study's observed interaction effects are consistent with the earlier findings, which found that combination variable interactions rather than a single component-controlled entrapment efficiency. The similar order of variable importance and the fit of the quadratic model in both studies validate the reproducibility and robustness of the Box-Behnken design strategy for optimizing lecithin-chitosan nanoparticle formulations and also show that similar mechanisms are at play in different drug-loaded systems using this carrier system [22].

Fourier Transform Infrared (FTIR) spectroscopy is an essential technique for identifying the functional groups present in a molecule. In Fig. 7c, FTIR spectra of pure DFP, the excipients (Chitosan, Lecithin, and Poloxamer 407), and the final DFP-CSLCNPs formulation were compared to assess chemical compatibility and the integrity of the components after nanoparticle preparation. The spectrum of the pure drug displayed characteristic peaks at 3373 cm^{-1} (N–H stretching), 2933 cm^{-1} (C–H stretching), and a prominent carbonyl stretch at 1737 cm^{-1}. The chitosan–lecithin system showed broad absorption around 3300 cm^{-1} (O–H/N–H stretching) and peaks at 2926 and 2856 cm^{-1} corresponding to aliphatic C–H groups. In the DFP-CSLCNPs formulation, the main functional group bands of the drug were preserved, with minor shifts and a reduction in intensity of the carbonyl peak, indicating successful encapsulation and potential interactions (e.g., hydrogen bonding) between the drug and polymer matrix. The absence of any new peaks suggests that there is no chemical incompatibility or degradation, confirming the stability and integrity of the nanoparticles.

The surface morphology of the DFP-CSLCNPs was analyzed using Scanning Electron Microscopy (SEM), which revealed spherical nanoparticles with smooth surfaces. The observed particle size was approximately 182.4 nm as shown in Fig. 7d, which closely corresponds with the values determined through dynamic light scattering (DLS) analysis presented in Fig. 7a. The uniform and smooth morphology indicates a well-formed polymer matrix and suggests controlled solvent diffusion during nanoparticle preparation.

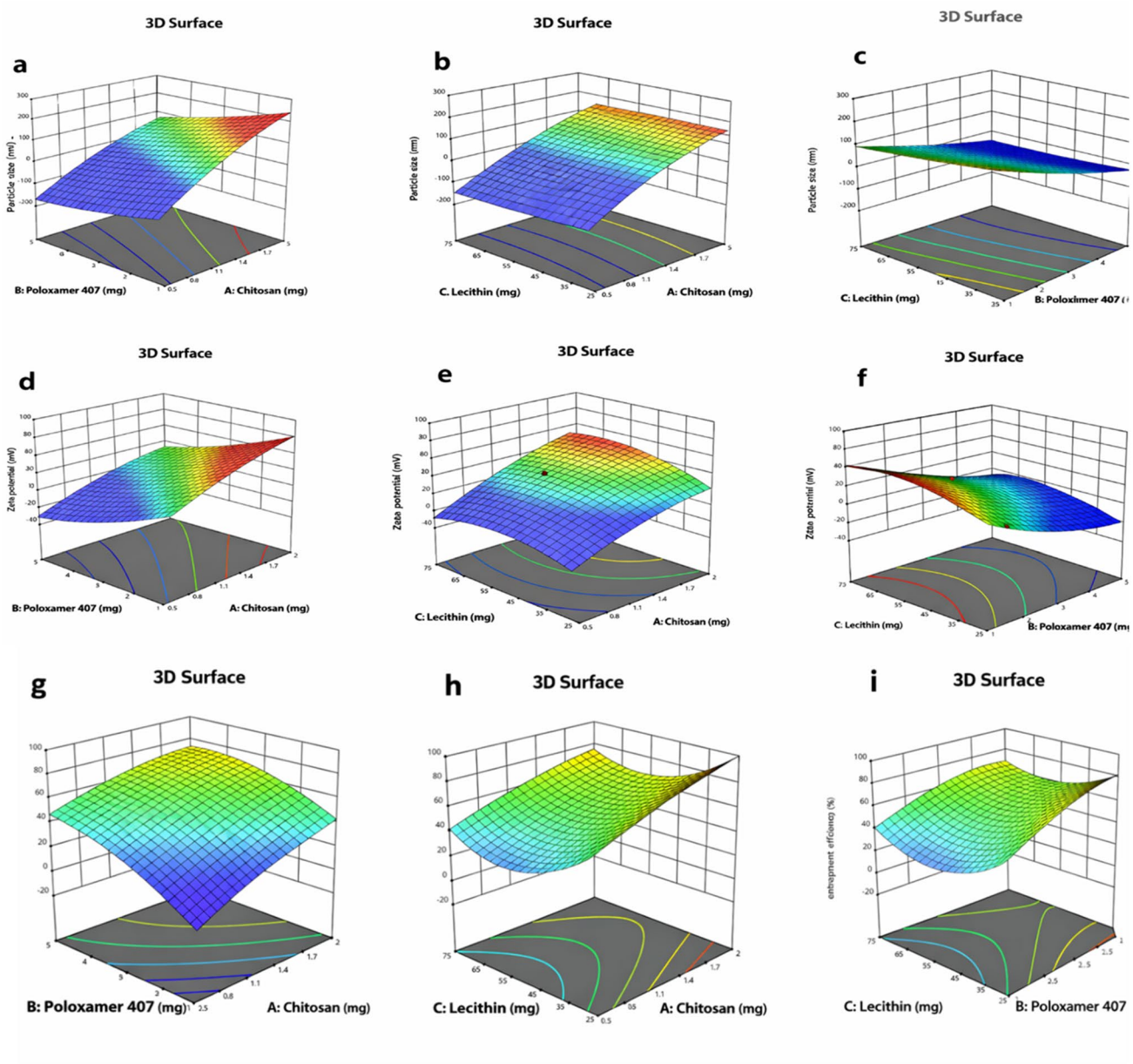

Fig. 5 3D Response Surface plots illustrating the interaction effects of formulation variables on the characteristics of DFP-CSLCNPs. **a** Chitosan and Poloxamer 407 on Particle Size (PS) (**b**) Chitosan and Lecithin on PS; (**c**) Poloxamer 407 and Lecithin on PS; (**d**) Chitosan and Poloxamer 407 on Zeta Potential (ZP); (**e**) Chitosan and Lecithin on ZP; (**f**) Poloxamer 407 and Lecithin on ZP; (**g**) Chitosan and Poloxamer 407 on Entrapment Efficiency (EE %); (**h**) Chitosan and Lecithin on EE (%); (**i**) Poloxamer 407 and Lecithin on EE (%)

Such characteristics are essential for achieving consistent particle size and promoting uniform drug release from the nanoparticles, confirming the effectiveness of the formulation process. Transmission Electron Microscopy (TEM) was used to examine the internal structure and size distribution of the optimized DFP-CSLCNPs formulation. Figure 7e, TEM images revealed spherical nanoparticles with smooth surfaces, confirming the uniform encapsulation of DFP within the polymer–lipid matrix and the homogeneous distribution of the particles [35, 36].

In Vitro Drug Release and Kinetics

DFP was released from optimized NPs and plain solution in a regulated manner for up to 24 h. As depicted in Fig. 8a, the DFP solution displayed a burst release, with 54.10 ± 0.13% of the drug released within 2 h, which can be attributed to its rapid solubilization under sink conditions. Nearly complete release was attained by 24 h. After 24 h, the percentage cumulative drug release (CDR) of the Form DFP-CSLCNPs reached 82.2 ± 2.71%. With an R^2 of 0.9699,

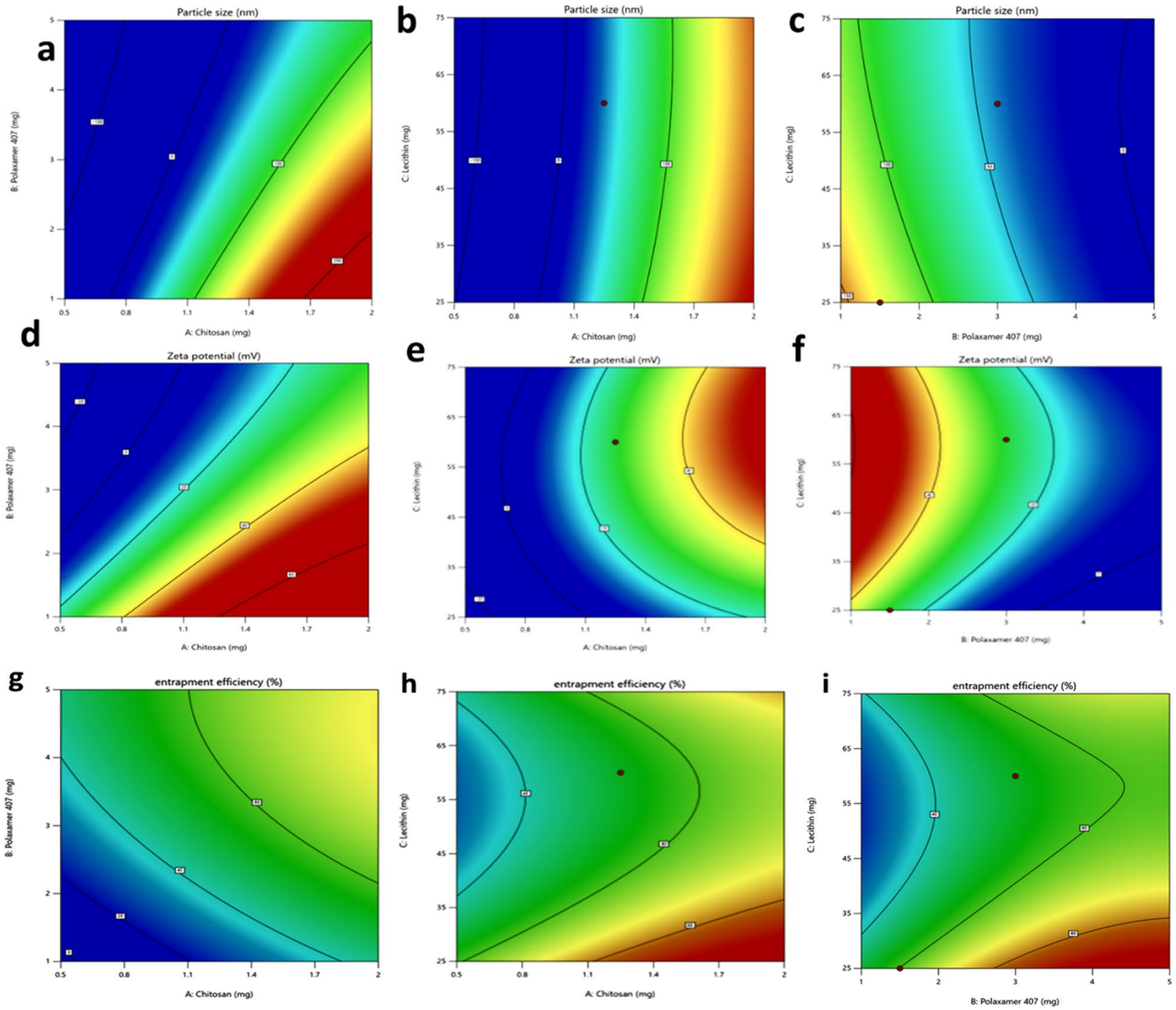

Fig. 6 2D Contour Plots illustrating the interaction effects of formulation variables on the characteristics of DFP-CSLCNPs. **a** Chitosan and Poloxamer 407 on Particle Size (PS) (**b**) Chitosan and Lecithin on PS; (**c**) Poloxamer 407 and Lecithin on PS; (**d**) Chitosan and Poloxamer 407 on Zeta Potential (ZP); (**e**) Chitosan and Lecithin on ZP; (**f**) Poloxamer 407 and Lecithin on ZP; (**g**) Chitosan and Poloxamer 407 on Entrapment Efficiency (EE %); (**h**) Chitosan and Lecithin on EE (%); (**i**) Poloxamer 407 and Lecithin on EE (%)

the drug release from DFP-CSLCNPs best resembled the Korsmeyer–Peppas model. The Higuchi model's R^2 was 0.9547, while the first-order model was 0.9004. Based on the curve-fitting analysis (Table 5), the release of DFP from the optimized DFP-CSLCNPs conformed to the Korsmeyer–Peppas model. This suggests that drug release from the nanoparticles is primarily governed by diffusion, following Fickian kinetics, as indicated by a release exponent (n) below 0.45. An R^2 value of 0.9547 for the Higuchi model indicates a very strong correlation between the experimental drug release data and the model's predictions, suggesting that the release of DFP from the CSLCNPs predominantly follows a diffusion-controlled mechanism, as described by the Higuchi equation. The observed release pattern suggests that the initial drug release is due to surface-adsorbed DFP, followed by a diffusion-controlled release from the polymer matrix. Drug release kinetics were assessed using multiple models, and the in vitro studies revealed a biphasic profile, characterized by an initial burst release succeeded by a sustained release phase. This behaviour can be attributed to the combined effects of the drug present on the nanoparticle surface and the drug encapsulated within the polymer matrix. This dual-phase release offers clinical benefits, particularly in MS treatment, where a rapid onset of action followed by prolonged therapeutic levels is desirable. These findings are particularly significant for intranasal formulations, where

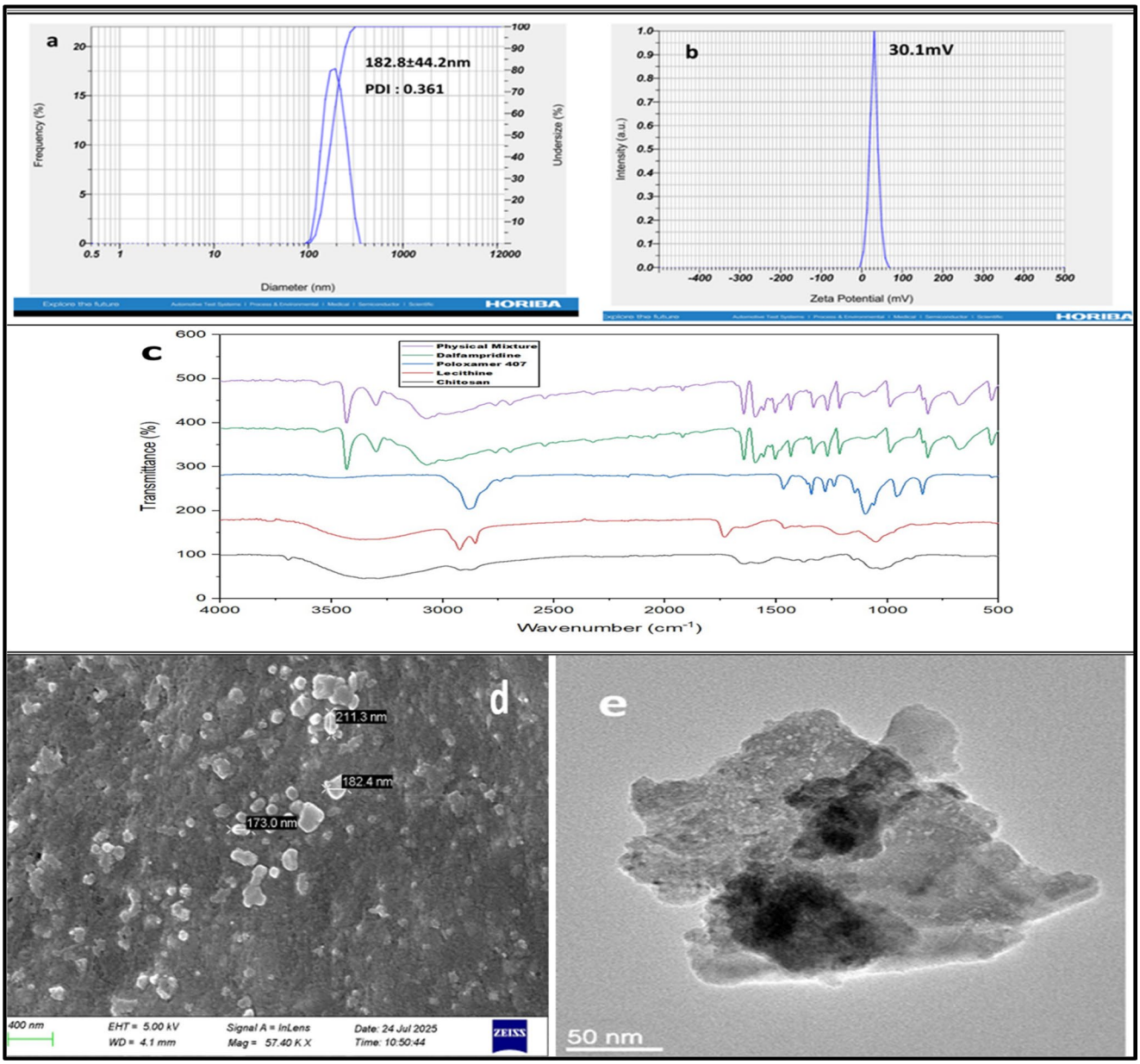

Fig. 7 (**a** & **b**) Physicochemical characterization of DFP-CSLCNP: Particle size distribution determined by dynamic light scattering (DLS) and Zeta potential, (**c**) Fourier Transform Infrared (FTIR) spectra, (**d** & **e**) Morphological characterization of optimized DFP-loaded chitosan–lecithin nanoparticles revealing internal structure and nanoscale dimensions of the particles: Scanning Electron Microscopy (SEM) image and Transmission Electron Microscopy (TEM) image

the nasal mucosa has limited residence time due to mucociliary clearance [37]. The results obtained by Paramita Saha et al. (2023), designed Rotigotine-loaded lecithin-chitosan nanoparticles (RTG-LCNPs) for intranasal administration, are in line with these findings. Diffusion-controlled drug release from a self-assembled lecithin-chitosan matrix was demonstrated by their formulation, which showed a controlled release profile based on the Korsmeyer-Peppas model. Similar to the current work, they also reported a biphasic release profile, with a burst release at the beginning and a continuous release later on. This was ascribed to the contributions of both the matrix-encapsulated and surface-bound drug amounts. The current DFP-CSLCNP formulation demonstrated a greater cumulative drug release of 82.2% in 24 h when compared to the current rotigotine LCNP formulation, suggesting comparatively more effective diffusion of the hydrophilic DFP from the nanoparticulate matrix. The sustained release phenomenon in both systems emphasizes the network-forming role of lecithin-chitosan interactions. In terms of clinical applications, the biphasic release pattern

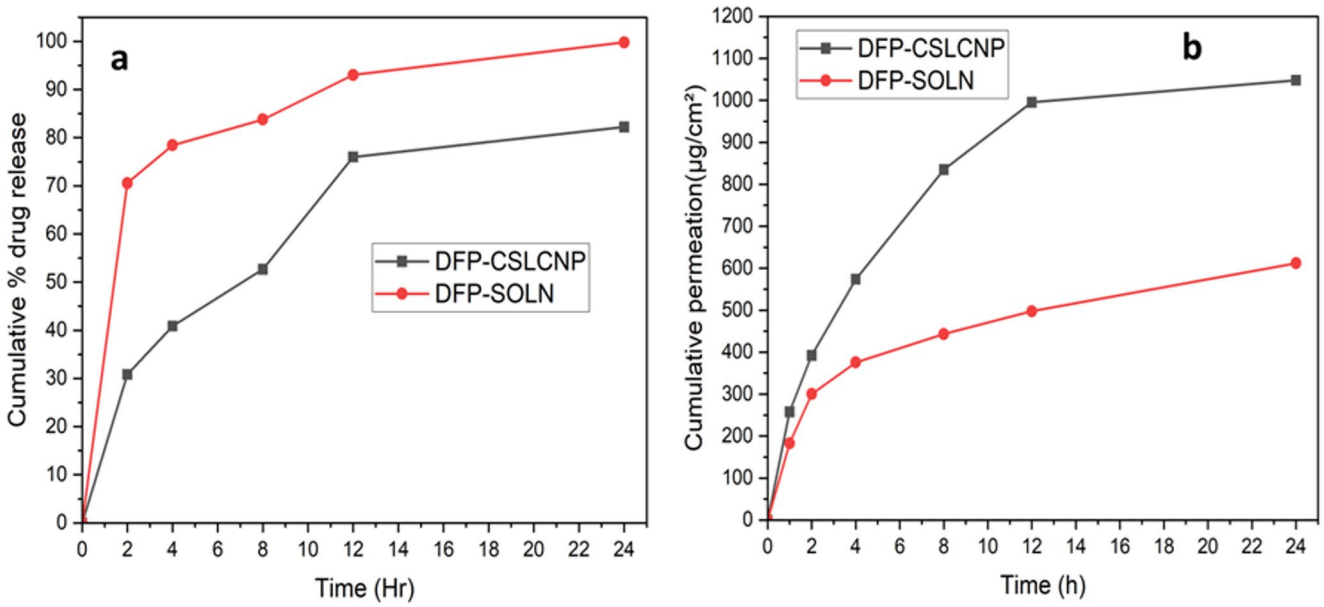

Fig. 8 (**a**) Cumulative % drug release profile (**b**) Ex vivo nasal permeation profile of DFP from Chitosan–Lecithin Nanoparticles (CSLCNPs) compared with plain DFP solution

Table 5 Correlation coefficient (R^2) values for the in vitro drug release kinetics of the optimized DFP-CSLCNPs formulation fitted to various mathematical models

Formulation	Zero order	First order	Higuchi Model	Hixon – Crowell	Korsmeyer–Peppas Model	
	R^2	R^2	R^2	R^2	R^2	n
DFP-CSLCNPs	0.7735	0.9004	0.9547	0.8672	0.9699	0.4183
DFP -SOLN	0.6098	0.9835	0.881	0.7861	0.6556	0.8018

is beneficial for intranasal delivery in MS therapy, where a rapid onset of action (attributable to the burst release effect) followed by a sustained therapeutic concentration is preferred. In addition, sustained release is especially valuable in intranasal formulations to overcome the rapid mucociliary clearance and improve drug retention time at the site of absorption. Accordingly, in comparison with the previously documented lecithin-chitosan nanoparticle delivery systems, the current formulation shows comparable release performance, while exhibiting promising sustained delivery properties for nose-to-brain targeting [17]. A sustained release mechanism ensures that therapeutic concentrations of the drug are maintained over a prolonged period, thereby reducing the need for frequent administration.

Ex Vivo Nasal Drug Permeation of DFP-CSLCNPs

After 24 h, DFP-CSLCNPs showed a significantly higher cumulative permeation across the nasal mucosa (1047.01 µg/cm²) than the plain drug solution (611.46 µg/cm²), as presented in Fig. 8b. The results clearly demonstrate the superior permeability of the nanoparticle formulation. The steady-state flux (Jss) and apparent permeability coefficient

Table 6 Ex vivo nasal permeation parameters of DFP from Chitosan–Lecithin Nanoparticles (DFP-CSLCNPs) compared with plain DFP solution (DFP-SOLN) across excised nasal mucosa

Formulation	Flux J_{ss} (µg/cm²/h)	P_{app} (cm/h×10^{-3})	Cumulative DFP Permeated (µg/cm²)
DFP-CSLCNPs	68.18 ± 3.41	68.16 ± 0.36	1047.01
DFP -SOLN	37.22 ± 1.86	37.24 ± 2.12	611.46

Data are expressed as mean ± SD (n = 3).

(Papp) of DFP were evaluated using an ex vivo Franz diffusion cell setup, with the results summarized in Table 6. The flux J_{ss} values for the DFP-loaded Chitosan–Lecithin Nanoparticles (DFP-CSLCNPs) and plain DFP solution were found to be 68.18 ± 3.41 µg/cm²/h and 37.22 ± 1.86 µg/cm²/h, respectively. Moreover, the nanoparticulate size (in the sub-200 nm range) ensures a larger surface area and better interaction with the mucosal surface. The optimized formulation showed sustained release behaviour, as evidenced by its controlled permeation profile over 24 h, which is favorable for prolonged therapeutic action and reduced dosing frequency. The limited permeation of DFP from the pure solution may also be attributed to its poor lipophilic

character. Overall, the significantly higher cumulative permeation ($p < 0.05$) of DFP from CSLCNPs compared to the plain solution confirms their potential in enhancing intranasal delivery and brain targeting for the management of MS. The permeation enhancement mechanism of DFP-CSLCNPs can be explained by the synergistic effect of the mucoadhesive and tight junction-opening properties of chitosan, in addition to the nanoscale particle size, which allows for better interaction with the nasal epithelium. These results are in strong agreement with the study published in Pharmaceutics by Paramita Saha et al.2023, which showed that lecithin-chitosan nanoparticles significantly enhanced the nasal permeability of Rotigotine compared to the drug suspension due to the increased interaction with the epithelium and the transient modulation of tight junctions. Similar to their results, the current formulation shows that its incorporation into a lecithin-chitosan nanocarrier system effectively overcomes the permeability limitations of the free drug. Moreover, the sustained permeation profile is in agreement with previously reported lecithin-chitosan systems, which supports the mucosal residence of the system for a longer period of time and enhances drug absorption. The comparative analysis confirms that the permeation enhancement mechanism of DFP-CSLCNPs is in agreement with the established evidence for chitosan-based nose-to-brain nanocarriers, thus reiterating their efficacy for intranasal brain targeting [17].

Naso Ciliotoxicity and Biocompatibility of DFP -CSLCNPs

Nasal safety was evaluated through histopathological examination of goat nasal mucosa following exposure to the test formulations. The intranasal route was selected to facilitate direct nose-to-brain delivery, potentially reducing systemic drug exposure and minimizing dose-related adverse effects. Local nasal safety was evaluated through a nasociliotoxicity study using goat nasal mucosa. Histopathological examination revealed preserved epithelial architecture, intact ciliary structure, and no evidence of significant inflammatory infiltration or mucosal erosion compared with the untreated control group. These observations indicate that the developed formulation was well tolerated in the nasal mucosa under the tested conditions. Histological examination of tissues exposed to the optimized DFP-CSLCNPs formulation demonstrated an intact epithelial structure with well-preserved cilia and an absence of epithelial disruption, inflammatory response, or cellular degeneration, as shown in Fig. 9. These observations were comparable to those in the untreated control group, confirming the absence of any ciliotoxicity or irritant effects. In contrast, the tissue samples from the group exposed to a higher concentration of the free drug exhibited mild epithelial thinning and vascular congestion, suggesting potential irritation at elevated doses. Collectively, these results confirm the non-irritant, biocompatible, and mucosa-safe nature of the DFP-CSLCNPs intranasal formulation, supporting its suitability for nasal drug delivery without

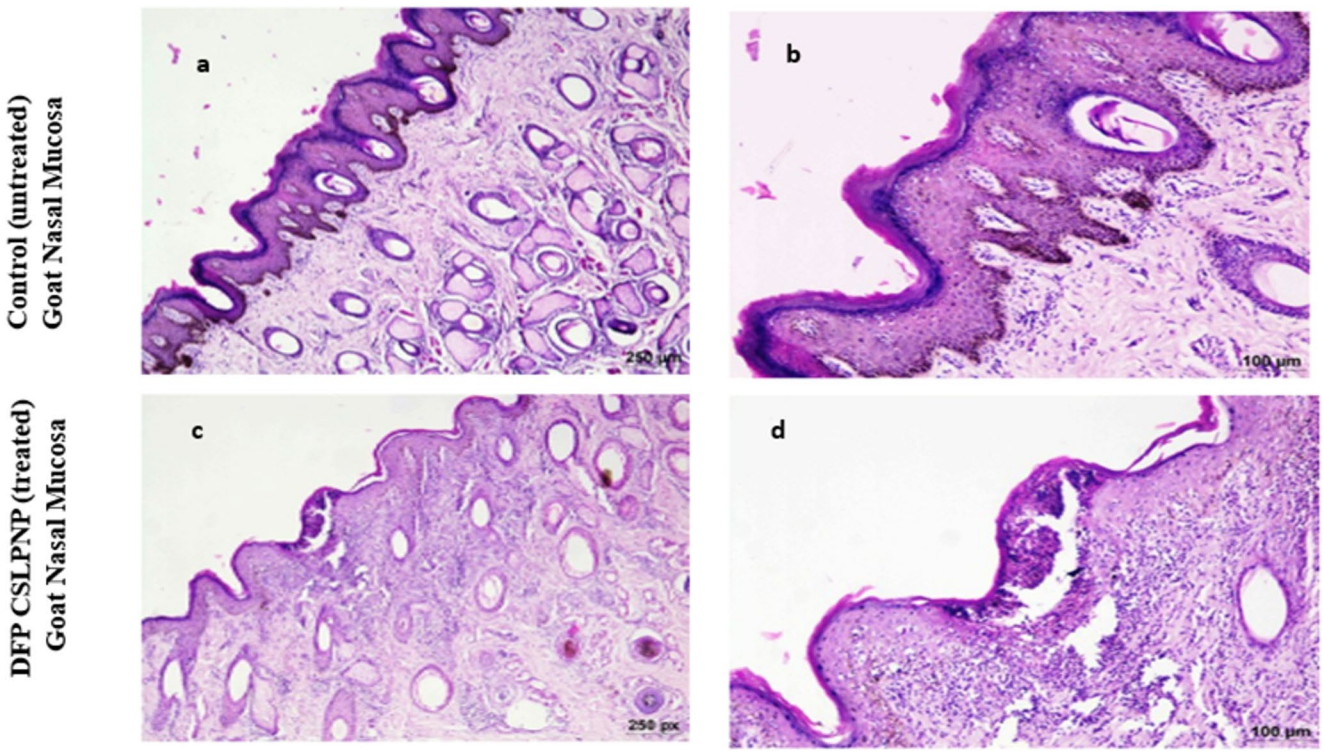

Fig. 9 Naso Ciliotoxicity and Biocompatibility of DFP- CSLCNPs - Histopathological images of goat nasal mucosa from the control group (**a** & **b**) and the DFP CSLCNPs group (**c** & **d**) showing within normal limits Haematoxylin & Eosin staining at 4X and 10X magnification

Table 7 Stability study of DFP-CSLCNP under different storage conditions

Parameter	0 Day	7th Day	15th Day	45th Day
Particle Size (nm)	184.23 ± 0.38	184.73 ± 0.15	186.87 ± 0.25	188.2 ± 0.26
PDI (%)	0.361 ± 012	0.358 ± 13	0.349 ± 002	0.378 ± 56
Zetapotential (mV)	30.13 ± 0.06	30.16 ± 0.06	31.23 ± 0.06	32.05 ± 0.21
Entrapment Efficiency (%EE)	82.3 ± 0.5	80 ± 0.004	79 ± 0.35	76.23 ± 023

compromising mucosal integrity. The non-toxic and non-irritant profile of the formulation is likely due to the use of biocompatible excipients, particularly chitosan and lecithin, both of which have been extensively studied and shown to exhibit minimal toxicity in mucosal tissues [38, 39].

Stability Study of DFP-CSLCNP

The optimized DFP-CSLCNPs formulations were subjected to accelerated stability testing for 45 days following ICH guidelines. During this period, the formulations were evaluated for physical appearance, particle size, zeta potential and entrapment efficiency (%EE). No significant changes were observed in any of the measured parameters, and all values remained within acceptable limits, as listed in Table 7. The DFP-CSLCNPs displayed sustained colloidal stability during the evaluation period, showing no detectable aggregation, precipitation, phase separation, or turbidity. This outcome confirms that the optimized formulation possesses remarkable stability under accelerated conditions, emphasizing its promise for extended shelf life and prospective clinical utilization. The stability profile of the optimized DFP-CSLCNPs is comparable to previously reported lecithin–chitosan and chitosan-coated lipid nanoparticle systems, where sustained particle size, maintained surface charge, and minimal loss of drug entrapment during storage were observed (Pardeike et al., 2009; Fonte et al., 2013). These studies similarly attribute enhanced stability to polymer–lipid interactions and electrostatic stabilization. In their research, the lyophilized nanoparticles showed physicochemical stability during refrigerated storage, with no significant change in particle size, zeta potential, and drug loading, indicating the efficient preservation of structural integrity of the self-assembled lipid-polymer matrix. The similar stability trend observed in the current formulation indicates that the strong electrostatic interactions between the positively charged chitosan and negatively charged lecithin play a significant role in preserving the colloidal stability and

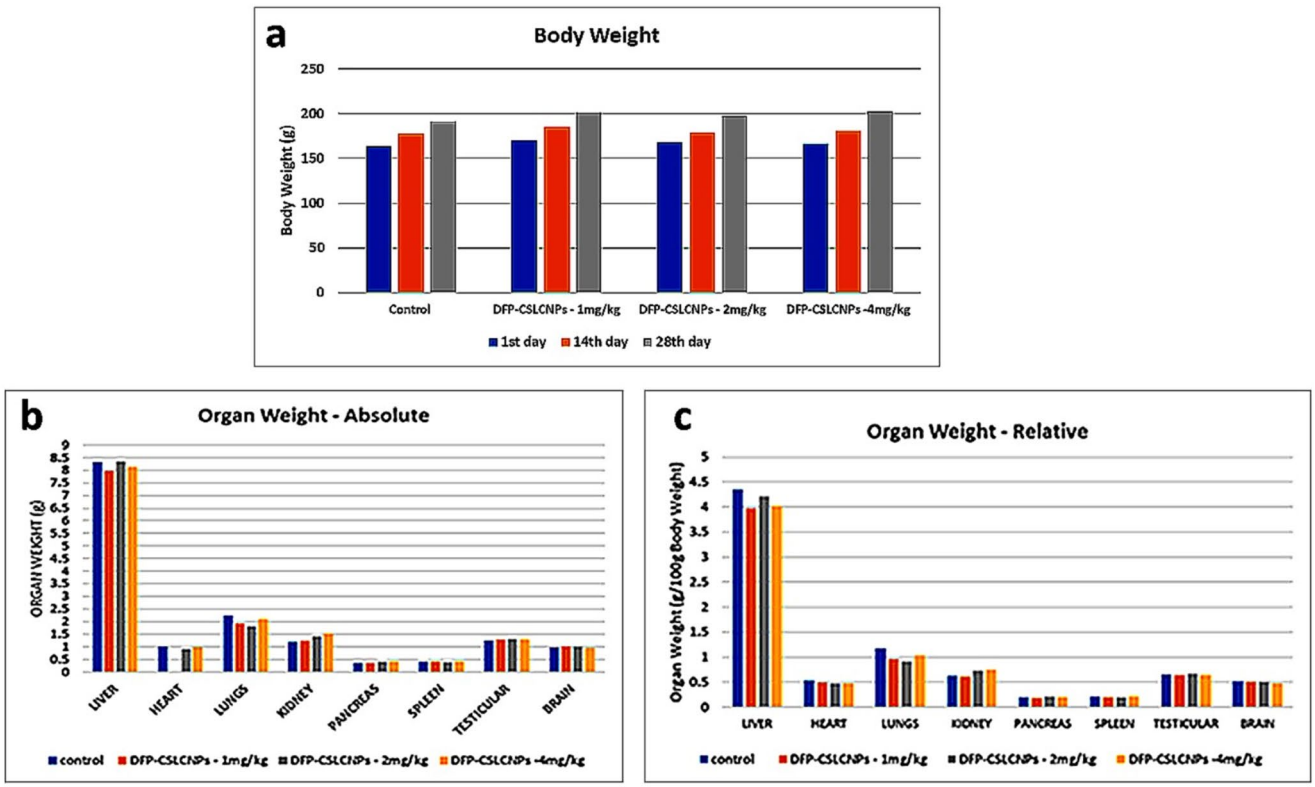

Fig. 10 Changes in body weight (**a**), absolute organ weights (**b**), and relative organ weights (**c**) of Wistar rats over 28 days following intranasal administration of DFP-CSLCNPs at doses of 1, 2, and 4 mg/kg compared with the control group. Values are expressed as mean ± SD ($n = 6$). $^{**}p < 0.01$ vs. control group

inhibiting aggregation. Additionally, the retention of entrapment efficiency under stress conditions indicates the robustness of the nanoparticulate core-shell structure, which resists drug leakage over time. Compared to the conventional polymeric nanoparticles that are known to exhibit instability under accelerated conditions, the lecithin-chitosan hybrid systems consistently exhibit enhanced structural resilience. Therefore, the current results are in good agreement with the existing literature, confirming that the CSLCNPs exhibit sufficient physicochemical stability for long-term storage and potential clinical applications in intranasal delivery systems [17].

Toxicological Assessment of DFP-CSLCNPs Formulation

In a 28-day subacute study, male Wistar rats received continuous intranasal doses of DFP-CSLCNPs. Four groups were established: one control group with a placebo and three treatment groups receiving low (1 mg/kg), medium (2 mg/kg), and high (4 mg/kg) doses. Throughout the study, animals were closely monitored for mortality and signs of toxicity. No deaths or significant adverse effects were observed in any groups. No clinical signs of toxicity, including nasal bleeding, ocular irritation, excessive blinking, nasal secretions, respiratory distress, or abnormal behaviours, were observed in the treated rats compared to controls ($p < 0.01$). These results suggest that intranasal administration of DFP-CSLCNPs is well-tolerated and does not produce observable gross toxicity, supporting its safety for nose-to-brain. During the study, food and water intake in the DFP-CSLCNPs-treated groups differed significantly from the control group ($p < 0.01$). Despite this, body weight gain, recorded using a calibrated digital balance, was consistent across all groups ($p < 0.01$). Figure 10a shows that rats treated with low, medium, and high

Table 8 Haematological parameters in male Wistar rats following 28 days of continuous administration of DFP-CSLCNPs at different dose levels

Treatment	Haematocrit (%)		Total WBC (Cells/Cumm)		Lymphocytes (%)	
	14th Day	28th Day	14th Day	28th Day	14th Day	28th Day
Control	27.32 ± 0.09	25.47 ± 0.08	5265 ± 66.52	5666 ± 03.6	92.17 ± 0.08	92.8 ± 0.098
DFP-CSLCNPs 1 mg/kg	27.15 ± 0.52**	26.3 ± 0.58*	5515 ± 215.3**	5598 ± 215.2**	92.20 ± 0.05*	93.3 ± 0.072**
DFP-CSLCNPs 2 mg/kg	27.12 ± 0.35**	27.97 ± 0.36*	5700 ± 257.1**	5730 ± 258.5**	92.9 ± 0.58*	93.2 ± 0.56**
DFP-CSLCNPs 4 mg/kg	27.20 ± 0.29**	27.32 ± 0.24*	5675 ± 183.3**	5783 ± 181.1**	93.80 ± 0.88*	94.8 ± 0.90**
Treatment	Polymorphs (%)		Eosinophils (%)		RBC (Cells/Cumm)	
	14th Day	28th Day	14th Day	28th Day	14th Day	28th Day
Control	3.03 ± 0.12	3.15 ± 0.08	4.27 ± 0.043	4.36 ± 0.071	7.17 ± 0.02	8.18 ± 0.02
DFP-CSLCNPs 1 mg/kg	3.08 ± 0.22**	3.28 ± 0.25*	4.08 ± 0.20*	4.42 ± 0.178**	7.36 ± 0.19*	7.99 ± 0.19**
DFP-CSLCNPs 2 mg/kg	3.57 ± 0.12**	3.70 ± 0.15**	4.43 ± 0.21**	4.75 ± 0.262**	7.43 ± 0.21**	8.48 ± 0.21**
DFP-CSLCNPs 4 mg/kg	3.35 ± 0.18**	3.58 ± 0.18**	4.78 ± 0.19**	4.93 ± 0.219**	7.06 ± 0.03**	8.98 ± 0.02**
Treatment	Platelet Count (cells/cumm)		Mean Cell Volume (*fl.*)		Mean Cell Haemoglobin(*pg*)	
	14th Day	28th Day	14th Day	28th Day	14th Day	28th Day
Control	6.74 ± 0.01	6.95 ± 0.013	38.17 ± 0.06	38.48 ± 0.12	18.4 ± 0.06	18.72 ± 0.06
DFP-CSLCNPs 1 mg/kg	5.93 ± 0.18**	5.25 ± 0.172**	37.90 ± 0.31*	38.05 ± 0.26*	18.5 ± 0.06*	18.72 ± 0.07**
DFP-CSLCNPs 2 mg/kg	6.42 ± 0.01**	6.46 ± 0.006**	36.90 ± 0.41**	37.08 ± 0.41**	18.1 ± 0.50**	19.0 ± 0.09**
DFP-CSLCNPs 4 mg/kg	5.96 ± 0.02**	5.46 ± 0.006**	38.40 ± 0.09*	39.62 ± 0.12**	18.4 ± 0.29**	19.57 ± 0.21**
Treatment	Haemoglobin (gms%)		Mean Erythrocyte (g/ dL)		Glucose (mg/dl)	
	14th Day	28th Day	14th Day	28th Day	14th Day	28th Day
Control	13.07 ± 0.14	13.35 ± 0.05	38.55 ± 0.17	38.85 ± 0.16	170.2 ± 3.22	168.4 ± 3.24
DFP-CSLCNPs 1 mg/kg	13.77 ± 0.13*	13.05 ± 0.13**	40.08 ± 1.67*	40.25 ± 1.63**	172.4 ± 2.30*	172.6 ± 2.28*
DFP-CSLCNPs 2 mg/kg	13.03 ± 0.33**	13.00 ± 0.32**	39.08 ± 0.32**	40.10 ± 0.31**	170.9 ± 1.75**	171.3 ± 1.68**
DFP-CSLCNPs 4 mg/kg	13.88 ± 0.21*	14.05 ± 0.18**	39.22 ± 0.35**	39.95 ± 0.32**	174.1 ± 4.27**	176.2 ± 4.26**

DFP-CSLCNPs: DFP-Loaded Chitosan Lecithin Nanoparticles

All values are expressed as mean ± standard deviation ($n = 6$).

Statistical analysis was performed using one-way ANOVA followed by Dunnett's post hoc test.

Differences were considered statistically significant at $p < 0.05$.

*$p < 0.05$ vs. control group; **$p < 0.01$ vs. control group

Table 9 Hepatic profile in male Wistar rats following 28 days of continuous administration of DFP-CSLCNPs at different dose levels

Treatment	ALT (U/L)		AST (U/L)	
	14th Day	28th Day	14th Day	28th Day
Control	125.1 ± 3.69	125.4 ± 3.67	53.14 ± 1.73	53.32 ± 1.68
DFP-CSLCNPs 1 mg/kg	129.2 ± 5.23*	128.2 ± 5.21*	50.45 ± 2.41*	52.49 ± 2.39*
DFP-CSLCNPs 2 mg/kg	129.8 ± 4.28*	130.9 ± 4.27*	58.56 ± 1.91*	59.64 ± 1.91*
DFP-CSLCNPs 4 mg/kg	132.2 ± 4.34*	133.4 ± 4.40*	53.07 ± 0.49*	56.03 ± 0.55*
Treatment	ALP (U/L)		Direct Bilirubin (mg/dl)	
	14th Day	28th Day	14th Day	28th Day
Control	642.6 ± 14.56	648 ± 14.58	10.65 ± 0.13	10.83 ± 0.02
DFP-CSLCNPs 1 mg/kg	601.1 ± 21.26*	608.3 ± 21.25*	10.74 ± 0.06*	10.83 ± 0.01*
DFP-CSLCNPs 2 mg/kg	673.7 ± 33.73*	677.8 ± 33.74*	10.75 ± 0.06**	10.91 ± 0.03*
DFP-CSLCNPs 4 mg/kg	640.6 ± 27.39*	648.7 ± 27.41*	0.53 ± 0.03**	0.56 ± 0.16**

DFP-CSLCNPs: DFP-Loaded Chitosan Lecithin Nanoparticles

All values are expressed as mean ± standard deviation ($n = 6$).

Statistical analysis was performed using one-way ANOVA followed by Dunnett's post hoc test.

Differences were considered statistically significant at $p < 0.05$.

*$p < 0.05$ vs. control group; **$p < 0.01$ vs. control group

Table 10 Lipid Profile in male Wistar rats following 28 days of continuous administration of DFP-CSLCNPs at different dose levels

Treatment	Cholesterol (mg/dl)		TGL (mg/dl)		VLDL (mg/dl)	
	14th Day	28th Day	14th Day	28th Day	14th Day	28th Day
Control	41.08 ± 1.39	46.21 ± 1.42	75.31 ± 1.42	77.74 ± 1.25	14.91 ± 0.27	15.15 ± 0.25
DFP-CSLCNPs 1 mg/kg	40.57 ± 0.53*	44.66 ± 0.37**	74.76 ± 1.18*	79.94 ± 1.15*	15.89 ± 0.28*	15.99 ± 0.23*
DFP-CSLCNPs 2 mg/kg	40.04 ± 1.62**	45.16 ± 1.67**	75.09 ± 1.01*	79.24 ± 0.96*	16.46 ± 0.19**	17.51 ± 0.20**
DFP-CSLCNPs 4 mg/kg	41.22 ± 0.87**	41.39 ± 0.72**	73.64 ± 2.29**	75.00 ± 2.16*	15.92 ± 0.61**	17.21 ± 0.58**

DFP-CSLCNPs: DFP-Loaded Chitosan Lecithin Nanoparticles

All values are expressed as mean ± standard deviation ($n = 6$).

Statistical analysis was performed using one-way ANOVA followed by Dunnett's post hoc test.

Differences were considered statistically significant at $p < 0.05$.

*$p < 0.05$ vs. control group; **$p < 0.01$ vs. control group

Table 11 Renal profile in male Wistar rats following 28 days of continuous administration of DFP-CSLCNPs at different dose levels

Treatment	Creatinine (mg/dl)		Urea (mg/dl)	
	14th Day	28th Day	14th Day	28th Day
Control	0.50 ± 0.021	0.51 ± 0.019	37.19 ± 0.77	37.32 ± 0.76
DFP-CSLCNPs 1 mg/kg	0.48 ± 0.031*	0.49 ± 0.028*	37.17 ± 1.59*	37.20 ± 1.59*
DFP-CSLCNPs 2 mg/kg	0.49 ± 0.022**	0.47 ± 0.019*	38.06 ± 1.43*	38.67 ± 1.43*
DFP-CSLCNPs 4 mg/kg	0.50 ± 0.022**	0.52 ± 0.023**	38.01 ± 1.37**	39.32 ± 1.36**

DFP-CSLCNPs: DFP-Loaded Chitosan Lecithin Nanoparticles

All values are expressed as mean ± standard deviation ($n = 6$).

Statistical analysis was performed using one-way ANOVA followed by Dunnett's post hoc test.

Differences were considered statistically significant at $p < 0.05$.

*$p < 0.05$ vs. control group; **$p < 0.01$ vs. control group

doses (Groups II–IV) displayed steady weight gain over 28 days, indicating normal growth. As shown in Fig. 10b and c, both absolute and relative organ weights were comparable to controls, confirming that intranasal DFP-CSLCNPs were well-tolerated and exhibited no adverse effects on major organs [40, 41].

Treatment with DFP-CSLCNPs led to observable changes in several hematological parameters, including Haematocrit (Hct), Red Blood Cells (RBCs), total White Blood Cells (WBCs), Lymphocytes, Polymorphs, Eosinophils, Platelet Count, Mean Corpuscular Volume (MCV), Mean Cell Hemoglobin (MCH), and Mean Erythrocyte, as well as in

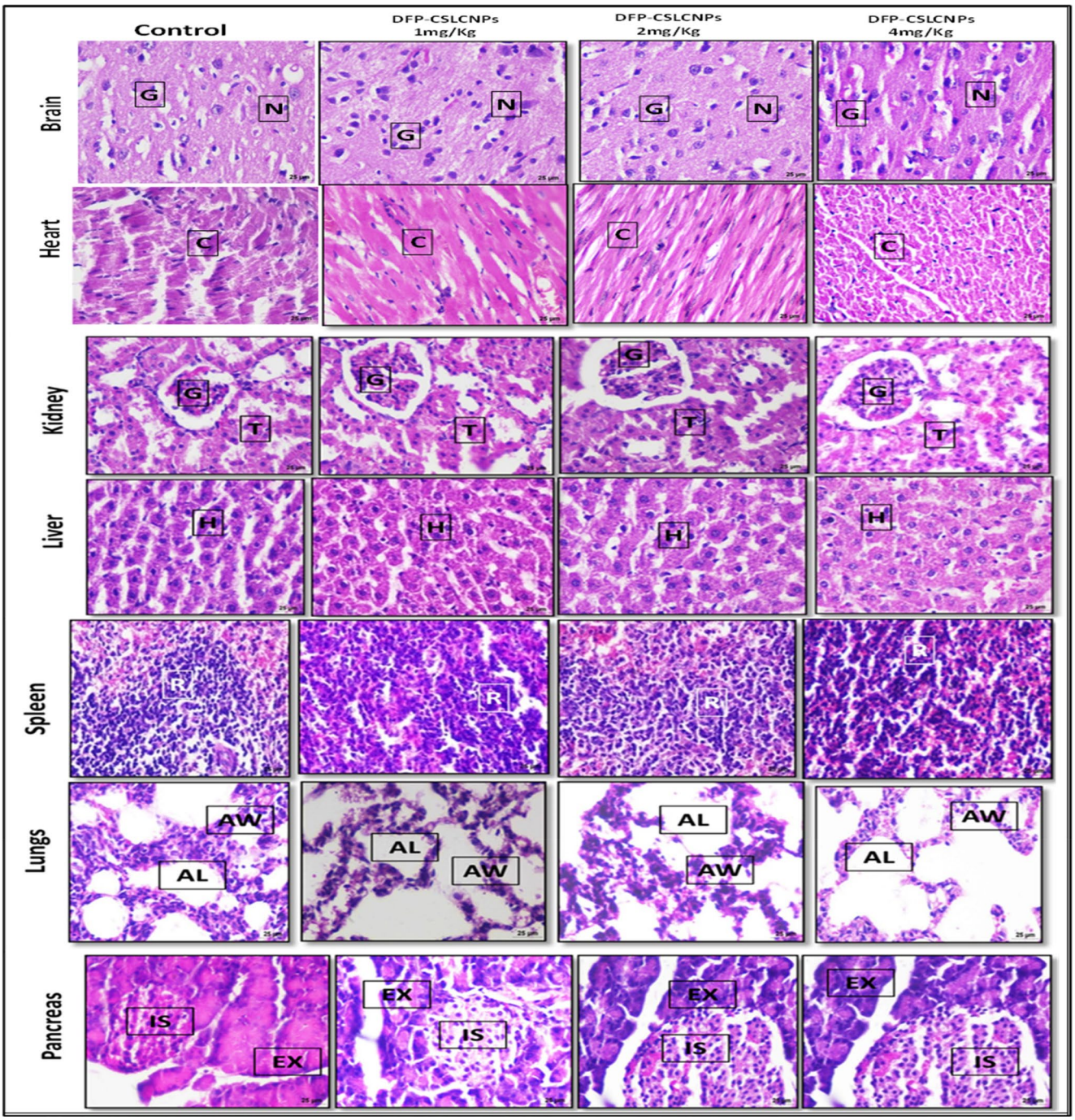

Fig. 11 Histopathological examination of major organs following subacute toxicity study of the DFP-CSLCNPs formulation showing Brain: Neurons (N) and Glial cells (G), Heart: Cardiac myocytes (C) with abundant eosinophilic cytoplasm, Kidney: Glomeruli (G) and Tubules (T), Liver: Hepatocytes (H), Spleen: Red pulp area (R), Lung: Alveoli Wall (Aw) and Alveolar Lumen (Al), Pancreas: Exocrine (Ex) and Islets (Is) with no significant pathological changes: Haematoxylin & Eosin staining at 10X magnification

serum glucose and total cholesterol levels (*$p<0.05$ and **$p<0.01$), as presented in Table 8.

Liver function markers such as AST, ALT, ALP, total bilirubin, total protein, and albumin also showed statistically significant differences in the treated groups compared with controls after 14 and 28 days (*$p < 0.05$ and **$p < 0.01$) as summarised in Table 9. Additionally, renal function and lipid profile analyses indicated significant changes in serum urea and creatinine levels following DFP-CSLCNP administration (*$p < 0.05$ and **$p < 0.01$) as detailed in Tables 10 and 11. Importantly, all measured values remained within normal physiological limits,

suggesting that the formulation did not cause renal or systemic toxicity [31, 42].

Histological examination of major organs from rats treated with DFP-CSLCNPs revealed no treatment-related abnormalities compared with the control group, as evident from Fig. 11. The brain tissue maintained normal architecture, with both neurons and glial cells appearing healthy and intact. Kidney sections showed well-preserved glomeruli and renal tubules with no evidence of structural changes. Examination of the spleen confirmed normal architecture, including intact red pulp regions and proper macrophage distribution. Heart tissue displayed normal morphology, characterized by intact cardiac muscle fibers, acidophilic cytoplasm, and centrally located nuclei, with no evidence of cellular degeneration or inflammation. These findings collectively indicate that intranasal administration of DFP-CSLCNPs for 28 days did not induce any histological toxicity in the evaluated organs.

Conclusion

This study successfully developed and optimized intranasal DFP-loaded Chitosan Lecithin nanoparticles (DFP-CSLCNPs) as a novel platform for brain-targeted delivery in the management of MS. Employing a Box–Behnken experimental design ensured precise optimization of critical formulation variables, yielding nanoparticles with desirable physicochemical attributes, small particle size (~182 nm), high zeta potential (+30.1 mV) and robust entrapment efficiency (>80%). The optimized formulation demonstrated sustained, diffusion-controlled drug release following Korsmeyer–Peppas kinetics, enhanced ex vivo nasal permeability, and superior flux compared to the plain drug solution, confirming its efficiency in promoting nose-to-brain transport. Comprehensive biocompatibility and safety evaluations, including histopathological, hematological, and biochemical assessments in Wistar rats, established the non-toxic and mucosa-safe profile of the formulation. Furthermore, the absence of systemic toxicity and maintained organ integrity underscore its suitability for chronic intranasal administration. The accelerated stability studies further confirmed the structural and functional integrity of the nanoparticles, highlighting their formulation stability under stress conditions. Collectively, these findings validate DFP-CSLCNPs as a safe, efficient, and stable intranasal nanocarrier system capable of overcoming BBB limitations and improving CNS drug bioavailability. This work establishes a strong preclinical foundation for translating DFP-CSLCNPs into advanced pharmacokinetic, biodistribution, and clinical evaluations aimed at enhancing therapeutic outcomes for patients with MS. Although the current study was able to successfully demonstrate the formulation optimization, safety, stability, and ex vivo nose-to-brain transport potential of DFP-CSLCNPs, there is a need for further research to enhance their translational potential. A thorough in vivo pharmacokinetic analysis with a focus on brain distribution would be an important next step. Furthermore, a biodistribution analysis with the aid of advanced imaging or analytical methods would help to identify the precise routes of transport and brain distribution.

Acknowledgements The authors sincerely acknowledge B.S. Abdur Rahman Crescent Institute of Science & Technology, Chennai, Tamil Nadu, India, and Cape Bio Lab and Research Centre, Marthandam, Tamil Nadu, India, for providing animal facilities and ethical support for the in vivo studies. The authors also extend their gratitude to the National Institute of Pharmaceutical Education and Research (NIPER), Kolkata, India, for offering the necessary facilities, technical assistance, and resources to carry out this research.

Author Contributions Jaghatha Therassama : Original draft preparation, methodology, resource provision, review and editing, supervision, and project administration. Jose Prakash Dharmian : Conceptualization, methodology, software validation, investigation, review, and editing. Justus Oliver Jaslin Edward : Methodology, formal analysis, data curation, and visualization. Somasundaram Arumugam : Formal analysis, investigation, and visualization. Pavazhaviji Pazhani: Software validation, investigation, and editing.

Funding This study did not receive any specific funding from public, commercial, or not-for-profit organizations.

Data Availability The datasets generated and/or analysed during the current study are available from the corresponding author upon reasonable request.

Declarations

Ethical Approval This study involved animal experiments performed by one of the authors and was approved by the Institutional Animal Ethics Committee of Cape Bio Lab & Research Centre, Tamil Nadu, India, under the ethical code CBLRC/IAEC/03/01-2025.

Competing interests The authors declare no competing interests.

References

1. Goodman AD, Brown TR, Krupp LB, Schapiro RT, Schwid SR, Cohen R. Sustained-release oral fampridine in multiple sclerosis: a randomized, double-blind, controlled trial. Lancet 2009; 373:732–738.
2. Patel S, Chavhan SS, Soni H, Babbar AK, Mathur R, Mishra AK, et al. Brain targeting of risperidone via intranasal route using lipid-based nanoparticles: formulation development, optimization, and biodistribution studies. Drug Deliv Transl Res. 2016;6:735–45.
3. Vandamme TF, Brobeck L. Poly(amidoamine) dendrimers as drug delivery systems: toxicological considerations. J Control Release. 2005;102:23–38.
4. Dinda SC, Pattnaik S, Panda SK, Bishi DK, Dinda A. Formulation and evaluation of mucoadhesive chitosan nanoparticles

for intranasal delivery of zolmitriptan. Asian J Pharm Clin Res. 2020;13:156–62.
5. Pires A, Fortuna A, Alves G, Falcão A. Intranasal drug delivery: how, why and what for? J Pharm Pharm Sci. 2009;12:288–311.
6. Illum L. Nasal drug delivery—possibilities, problems and solutions. J Control Release. 2003;87:187–98.
7. Jain R, Jain D, Kumar K, Jain N, Chourasia MK. Nose-to-brain delivery of antidepressant active constituents: a novel approach for treating depression. Curr Pharm Des. 2021;27:796–807.
8. Shende P, Deshmukh K, Trotta F. Drug delivery to the brain using nanotechnology. Pharmaceutics. 2021;13:2045.
9. Kumari A, Yadav SK, Yadav SC. Biodegradable polymeric nanoparticles based drug delivery systems. Colloids Surf B Biointerfaces. 2010;75:1–18.
10. Anselmo AC, Mitragotri S. Nanoparticles in the clinic: an update. Bioeng Transl Med. 2019;4:e10143.
11. Mukherjee A, Waters AK, Kalyan P, Achrol AS, Kesari S, Yenugonda VM. Lipid–polymer hybrid nanoparticles as a next-generation drug delivery platform: state of the art, emerging technologies, and perspectives. Int J Nanomed. 2019;14:1937–52.
12. Rawal T, Parmar R, Tyagi RK, Butani S. Resveratrol-loaded solid lipid nanoparticles for nose-to-brain delivery for the treatment of depression. Drug Deliv Transl Res. 2018;8:1230–42.
13. Salatin S, Barar J. Barriers to and strategies for effective drug delivery to the central nervous system. J Clin Pharmacol. 2020;60:1039–51.
14. Tzachev C, Danova S, Genova I, Tzacheva I. Chitosan-based delivery systems for intranasal administration of therapeutic agents. J Drug Deliv Sci Technol. 2021;61:102105.
15. Al-Ghananeem AM, Crooks PA. Nasal drug delivery of CNS-active drugs: pharmacokinetic considerations. Drug Deliv Transl Res. 2011;1:1–8.
16. Murthy A, Ravi PR, Kathuria H, Vats R. Self-assembled lecithin-chitosan nanoparticles improve the oral bioavailability and alter the pharmacokinetics of raloxifene. Int J Pharm. 2020;588. https://doi.org/10.1016/j.ijpharm.2020.119731.
17. Saha P, Singh P, Kathuria H, Chitkara D, Pandey MM. Self-assembled Lecithin-Chitosan nanoparticles improved rotigotine nose-to-brain delivery and brain targeting efficiency. Pharmaceutics. 2023;15. https://doi.org/10.3390/pharmaceutics15030851.
18. Gajra B, Dalwadi C, Patel R. Formulation and optimization of itraconazole polymeric lipid hybrid nanoparticles (Lipomer) using box behnken design. DARU J Pharm Sci. 2015;23. https://doi.org/10.1186/s40199-014-0087-0.
19. Gadhave DG, Kokare CR. Nanostructured lipid carriers engineered for intranasal delivery of teriflunomide in multiple sclerosis: optimization and in vivo studies. Drug Dev Ind Pharm. 2019;45:839–51. https://doi.org/10.1080/03639045.2019.1576724.
20. Auwal SM, Zarei M, Tan CP, Basri M, Saari N. Enhanced physicochemical stability and efficacy of angiotensin I-converting enzyme (ACE) - Inhibitory biopeptides by chitosan nanoparticles optimized using Box-Behnken design. Sci Rep. 2018;8. https://doi.org/10.1038/s41598-018-28659-5.
21. Saha P, Singh P, Kathuria H, Chitkara D, Pandey MM. Self-Assembled Lecithin-Chitosan Nanoparticles Improved Rotigotine Nose-to-Brain Delivery and Brain Targeting Efficiency. Pharmaceutics. 2023;15:851. https://doi.org/10.3390/pharmaceutics15030851.
22. Walbi IA, Ahmad MZ, Ahmad J, Algahtani MS, Alali AS, Alsudir SA, Aodah AH, Albarqi HA. Development of a Curcumin-Loaded Lecithin/Chitosan nanoparticle utilizing a box-behnken design of experiment: formulation design and influence of process parameters. Polym (Basel). 2022;14. https://doi.org/10.3390/polym14183758.
23. Gadhave DG, Kokare CR. Nanostructured lipid carriers engineered for intranasal delivery of teriflunomide in multiple sclerosis: optimization and *in vivo* studies. Drug Dev Ind Pharm. 2019;45:839–51. https://doi.org/10.1080/03639045.2019.1576724.
24. Safwat SM, El Tohamy M, Aboonq MS, Alrehaili A, Assinnari AA, Bahashwan AS, ElGendy AA, Hussein AM. Vanillic Acid Ameliorates Demyelination in a Cuprizone-induced multiple sclerosis rat model: possible underlying mechanisms. Brain Sci. 2024;14. https://doi.org/10.3390/brainsci14010012.
25. Tzankova V, Aluani D, Kondeva-Burdina M, Yordanov Y, Odzhakov F, Apostolov A, Yoncheva K. Hepatoprotective and antioxidant activity of quercetin loaded chitosan/alginate particles in vitro and in vivo in a model of paracetamol-induced toxicity. Biomed Pharmacother. 2017;92:569–79. https://doi.org/10.1016/j.biopha.2017.05.008.
26. Pokharkar V, Patil-Gadhe A, Palla P. Efavirenz loaded nanostructured lipid carrier engineered for brain targeting through intranasal route: In-vivo pharmacokinetic and toxicity study. Biomed Pharmacother. 2017;94:150–64. https://doi.org/10.1016/j.biopha.2017.07.067.
27. Pazhani P, Dharmian JP, Arumugam S, Pazhani P, Medapati VVP. Edoxaban enfolded beta-1,4-poly-d-glucosamine nanoparticles for targeting eponym Stuart–Prower factor for treatment of venous thrombosis. J Drug Target. 2024;32:1125–38. https://doi.org/10.1080/1061186X.2024.2377611.
28. Abdulredha FH, Mahdi MF, Khan AK. In silico evaluation of binding interaction and ADME study of new 1,3-diazetidin-2-one derivatives with high antiproliferative activity. J Adv Pharm Technol Res. 2023;14:176–84. https://doi.org/10.4103/JAPTR.JAPTR_116_23.
29. Yousfan A, Al Rahwanji MJ, Hanano A, Al-Obaidi H. A Comprehensive Study on Nanoparticle Drug Delivery to the Brain: Application of Machine Learning Techniques. Mol Pharm. 2024;21:333–45. https://doi.org/10.1021/acs.molpharmaceut.3c00880.
30. Formica ML, Real DA, Picchio ML, Catlin E, Donnelly RF, Paredes AJ. On a highway to the brain: A review on nose-to-brain drug delivery using nanoparticles. Appl Mater Today. 2022;29:101631. https://doi.org/10.1016/j.apmt.2022.101631.
31. Rai M, Singh AV, Paudel N, Kanase A, Falletta E, Kerkar P, Heyda J, Barghash RF, Pratap Singh S, Soos M. Herbal concoction Unveiled: A computational analysis of phytochemicals' pharmacokinetic and toxicological profiles using novel approach methodologies (NAMs). Curr Res Toxicol. 2023;5:100118. https://doi.org/10.1016/j.crtox.2023.100118.
32. Sączewski J, Popenda Ł, Fedorowicz J. In Silico SwissADME Analysis of Antibacterial NHC–Silver Acetates and Halides Complexes. Appl Sci. 2024;14:8865. https://doi.org/10.3390/app14198865.
33. Dalbanjan NP, Korgaonkar K, Eelager MP, Gonal BN, Kadapure AJ, Arakera SB, Kumar SK P. In-silico strategies in nano-drug design: Bridging nanomaterials and pharmacological applications. Nano TransMed. 2025;4:100091. https://doi.org/10.1016/j.ntm.2025.100091.
34. Gandhi S, Shastri DH, Shah J, Nair AB, Jacob S. Nasal delivery to the brain: harnessing nanoparticles for effective drug transport. Pharmaceutics. 2024;16. https://doi.org/10.3390/pharmaceutics16040481.
35. Jain A, Jain SK. In vitro and cell uptake studies for targeting of ligand anchored nanoparticles for colon tumors. Eur J Pharm Sci. 2015;65:70–8.
36. Kostrzynska M, Bachand A, Poupard P, Ryu G, Tsao R. In vitro screening for the potential cytotoxicity of the medicinal plant extracts using the mammalian fibroblast cell line Balb/c 3T3. Toxicol Vitro. 2007;21:929–42.
37. Shah B, Khunt D, Bhatt H, Misra M, Padh H. Application of central composite design to develop and optimize lecithin/chitosan

nanoparticles of curcumin for intranasal delivery. J Drug Deliv Sci Technol. 2016;31:110–7.
38. Ugwoke MI, Agu RU, Verbeke N, Kinget R. Nasal mucoadhesive drug delivery: background, applications, trends and future perspectives. Adv Drug Deliv Rev. 2005;57:1640–65.
39. Aungst BJ. Absorption enhancers: applications and advances. AAPS J. 2012;14:10–8.
40. Omidian H, Gill EJ, Dey Chowdhury S, Cubeddu LX. Chitosan Nanoparticles for Intranasal Drug Delivery. Pharmaceutics. 2024;16:746. https://doi.org/10.3390/pharmaceutics16060746.
41. Huang Q, Chen X, Yu S, Gong G, Shu H. Research progress in brain-targeted nasal drug delivery. Front Aging Neurosci. 2024;15. https://doi.org/10.3389/fnagi.2023.1341295.
42. Xinchen Y, Jing T, Jiaoqiong G. Lipid-based nanoparticles via nose-to-brain delivery: a mini review. Front Cell Dev Biol. 2023;11. https://doi.org/10.3389/fcell.2023.1214450.